

63 16428

Code-1

TECHNICAL NOTE

D-1809

AERODYNAMIC EFFECTS OF
MODIFYING WING INBOARD TRAILING-EDGE CAMBER OF A
MODEL AT HIGH SUBSONIC SPEEDS

By Richard J. Re

Langley Research Center
Langley Station, Hampton, Va.

NATIONAL AERONAUTICS AND SPACE ADMINISTRATION
WASHINGTON

May 1963

7
ode-1

CASE FILE 100-1

NATIONAL AERONAUTICS AND SPACE ADMINISTRATION

TECHNICAL NOTE D-1809

AERODYNAMIC EFFECTS OF
MODIFYING WING INBOARD TRAILING-EDGE CAMBER OF A
MODEL AT HIGH SUBSONIC SPEEDS

By Richard J. Re

SUMMARY

16422

An investigation has been made to determine the effect of a modification in the effective camber of the inboard wing sections near the trailing edge on the longitudinal aerodynamic characteristics of a model. The wing had discontinuous sweep at the leading edge with quarter-chord sweep of 40° on the outboard portion. The wing was modified near the trailing edge so that the camber lines near the body were reflexed and merged with the original camber lines at the midsemispan. The wing was tested with contoured, cylindrical, and modified cylindrical body configurations. The contoured body configuration was tested with and without horizontal and vertical tails. The Mach number of the test ranged from 0.40 to 0.96 and the angle of attack ranged from -5° to 15° . Reynolds number per foot varied from 2.6×10^6 to 4.4×10^6 .

The modified wing trailing edge generally reduced the drag coefficient at low lift coefficients but increased the drag coefficient in the range of lift coefficients for maximum lift-drag ratio and resulted in lower values of maximum lift-drag ratio. The modification alleviated model pitch-up which occurred at a lift coefficient of about 0.45 at Mach numbers of 0.92, 0.94, and 0.96. In addition, the modified trailing edge increased the model angle of zero lift about 1° at all Mach numbers and decreased the model pitching moment at zero angle of attack at all Mach numbers below 0.96.

INTRODUCTION

Some approaches to the design of efficient high-subsonic-speed transport airplane configurations are discussed in references 1 to 5. Among the devices and methods used to improve the efficiency of wing-body configurations at high subsonic speeds are the area-rule concept, body contouring, volume additions to the body, the addition of special bodies to the wings, and wing inboard leading-edge extensions.

The results of reference 1 indicate that shock-induced flow separation on the wing upper surface could be alleviated by the addition of leading-edge extensions to the inboard portion of the wing which reduced the inboard camber. The present investigation was conducted to determine the effect of a further reduction of inboard camber in the vicinity of the wing trailing edge. Thus, the wing of reference 1 with its inboard leading-edge extensions has been modified by decreasing the amount of camber near the trailing edge of the wing as far outboard as the midsemispan. This trailing-edge camber reduction, which in effect reduced the wing local angle of attack, included reflexing some of the camber lines near the body.

The wing was tested with contoured, cylindrical, and modified cylindrical bodies. In addition, horizontal-tail effectiveness was determined for the configuration with the contoured body. Tests were conducted at Mach numbers from 0.40 to 0.96 and at angles of attack from -5° to 15° . Reynolds number per foot varied from 2.6×10^6 to 4.4×10^6 .

SYMBOLS

b	wing span, ft
C_D	drag coefficient, $\frac{\text{Drag}}{qS}$
$C_{D,\min}$	minimum drag coefficient
C_L	lift coefficient, $\frac{\text{Lift}}{qS}$
C_{L_α}	lift-curve slope, per deg
C_m	pitching-moment coefficient about quarter-chord point of \bar{c} , $\frac{\text{Pitching moment}}{qS\bar{c}}$
C_{mC_L}	static longitudinal stability parameter
$C_{m_{i_t}}$	horizontal-tail effectiveness parameter, per deg
$C_{p,b}$	base pressure coefficient, $\frac{P_b - P_\infty}{q}$
c	local wing chord, measured streamwise, ft
\bar{c}	mean aerodynamic chord of wing without leading-edge extension, 1.097 ft
\bar{c}_t	mean aerodynamic chord of horizontal tail, 0.693 ft
i_t	angle of incidence of horizontal tail, deg

$(L/D)_{\max}$	maximum lift-drag ratio
M	free-stream Mach number
P_b	static pressure at model base, lb/sq ft
p_{∞}	free-stream static pressure, lb/sq ft
q	free-stream dynamic pressure, lb/sq ft
S	area of wing without leading-edge extension, 8 sq ft
x/c	nondimensional streamwise coordinate from wing leading edge (positive downstream)
$\frac{y}{b/2}$	nondimensional spanwise coordinate from body center line
z/c	nondimensional vertical coordinate from wing leading edge (positive upward)
α	angle of attack of body reference line, deg

MODEL AND APPARATUS

Models

A photograph showing the model sting-mounted in the test section of the wind tunnel is presented as figure 1. Sketches presenting geometric details of the various model components are presented in figure 2.

Wing.- The basic unmodified wing of reference 1 had an aspect ratio of 8, a taper ratio of 0.3, 40° of sweepback at the wing quarter-chord line, and NACA 65A-series airfoil sections perpendicular to the quarter-chord line. The wing was twisted and cambered for $C_L = 0.514$ by using linear theory for the special case of sonic velocity as given in the appendix of reference 1. Streamwise thickness-chord ratio for the wing before the inboard leading-edge chord extensions were added varied from 0.12 at the root to 0.06 at the 0.60-semispan station and was constant from that station to the wing tip.

The wing inboard leading-edge extension planform was made by extending the wing root chord at the body center line 19.1 percent and forming a new wing leading-edge apex by connecting this point to the original wing leading edge at the midsemispan. A new, essentially uncambered, leading edge was then formed by a streamwise distribution of NACA 65A-series airfoil sections about straight lines tangent to the original section camber lines at the point of maximum thickness. Fairing of the wing surfaces was required to a small extent since the 65A-sections

of the extension were applied streamwise and the 65A-sections of the original wing were applied perpendicular to the quarter chord. The maximum thicknesses of the wing sections were not changed. The inboard leading-edge extension was evaluated in the tests of reference 1 and remained an integral part of the wing throughout the current investigation.

A modification to the inboard trailing-edge camber lines of the wing with leading-edge extensions was applied in the area aft of a line connecting a point on the body center line 28.10 percent of the root chord forward of the trailing edge with the wing trailing edge at the midsemispan. (See fig. 3.) The new wing camber lines were reflexed near the wing root and merged with the original camber lines at the midsemispan. No attempt was made to retain the original design lift coefficient (0.514) or spanwise load distribution for the wing with either the leading-edge extensions or the trailing-edge modification.

Bodies.- Two different bodies were used in the tests. One was a modified version of a body that was indented according to the area rule and then contoured to be compatible with the streamlines at the wing root for $C_L = 0.514$ on the original wing. Modification to this body consisted of removing volume in the vicinity of its maximum cross section and adding volume at its minimum area station near the wing root to lessen the amount of indentation and contouring. Cross sections of the contoured body are shown in figure 4, and an area distribution for the body and wing is shown in figure 5. The second body that was used was tested with and without a modification. This body had circular cross sections back to station 60 with the rearward part becoming elliptic in cross section to provide sting clearance within the model. The nose was an ellipsoid of revolution of fineness ratio 3.577. A modification, similar to modifications used in references 2 and 5, was made to this body. This modification consisted of an addition of volume to the top of the fuselage forward of the wing and was designed for the model without the wing leading-edge extension. An area distribution for the wing with inboard leading-edge extensions and the modified cylindrical body is shown in figure 6. Both cylindrical and contoured bodies had a base area of 14.71 square inches.

Horizontal and vertical tails.- The horizontal tail had an aspect ratio of 4.0, taper ratio of 0.3, and streamwise NACA 65A006 airfoil sections. Horizontal-tail incidences of -1° and 2° could be set. The vertical tail had an aspect ratio of 1.25, taper ratio of 0.3, and streamwise NACA 65A006 airfoil sections. Sketches of the tails are included in figure 2.

Apparatus

The investigation was made in the Langley 16-foot transonic tunnel, which is an atmospheric single-return wind tunnel with an octagonal slotted test section. The model was supported on a sting-support system and was kept near the tunnel center line throughout the angle-of-attack range.

Model forces and moments were measured with an internal six-component strain-gage balance. Model angle of attack was determined with a pendulum-type strain-gage inclinometer located inside the model nose. An average base pressure was

obtained from three manifolded pressure tubes on the sting just inside the model base.

TESTS

All configurations were tested in the Mach number range of 0.40 to 0.96 with a Reynolds number per foot variation of about 2.6×10^6 to 4.4×10^6 . Model angle of attack was within the range -5° to 9° for all Mach numbers except 0.40 at which 15° was the upper limit.

The wing was tested with the contoured body with and without tail surfaces. The settings of the horizontal-tail incidence angles were -1° and 2° . The cylindrical and modified cylindrical body configurations were tested without horizontal and vertical tails. In addition, the cylindrical body was tested without the wing.

A contoured body configuration was tested with fixed and free transition to determine the effect of transition on the model aerodynamic characteristics. All other tests were conducted with fixed transition on the body nose and the wing. Transition was fixed by means of 0.125-inch-wide strips of No. 180 carborundum grains placed around the nose at 2.5 percent of the body length and at 2.5 percent of the local chord line on both upper and lower surfaces of the wing. The results obtained with the model configuration having the unmodified wing inboard trailing edge were reported in reference 1, and were obtained with transition fixed by means of strips of No. 220 carborundum grains. Boundary-layer transition was not fixed on the horizontal or vertical tail.

The body base pressure coefficients presented in figure 7(a) for the model with and without the inboard trailing-edge camber modification to the wing show a small but consistent difference which, it is believed, cannot wholly be attributed to the change in model configuration. The data for the configuration with the unmodified trailing edge were obtained during the tests of reference 1 in the Langley 16-foot transonic tunnel before a test-section slot-shape modification was made. The installation of auxiliary plenum suction to increase the speed capability of the tunnel necessitated the slot modification to maintain acceptable test-section center-line pressure distributions with the suction system operating at Mach numbers above 1.10. A comparison of tunnel-calibration center-line pressure distributions for the two test-section slot shapes shows no significant differences in the range of subsonic Mach numbers of the present investigation. The difference in base pressure coefficient at $C_L = 0$ amounts to 0.0008 in drag coefficient at $M = 0.40$ and 0.0005 at $M = 0.96$; both values are within the limits of accuracy of the drag data.

CORRECTIONS AND ACCURACY

All force data presented have been adjusted to the condition of free-stream static pressure existing at the model base. Values of the pressure coefficient

measured at the model base are presented in figure 7. No other corrections or adjustments to the data have been made.

The Mach number was accurate within ± 0.01 and the angle of attack was accurate within $\pm 0.1^\circ$. The accuracy of the data based on instrument error is estimated to be within the following limits:

	M = 0.40	M = 0.80
C_L	± 0.012	± 0.005
C_D at $C_L = 0$	± 0.0015	± 0.0006
C_m	± 0.0023	± 0.0009

RESULTS AND DISCUSSION

The effect of fixing boundary-layer transition is shown in the basic-data plots of figure 8 and the summary-data plots of figure 9 for the model with the contoured body, horizontal tail ($i_t = -1^\circ$), and vertical tail. Of particular interest is the effect shown on the pitching-moment data of figure 8(c) where a decrease of model stability due to fixed transition is indicated at low positive lift coefficients. This effect is further illustrated in the summary data of figure 9(b) where the static longitudinal stability parameter C_{mC_L} is plotted

for the model with fixed and free transition. The lift data of figure 8(a) show that at positive lift coefficients, the lift-curve slopes for the model with fixed transition were reduced at Mach numbers from 0.84 to 0.96. In the drag data of figure 8(b) it will be seen that the drag of the model with fixed transition was generally greater than that of the model with free transition at all Mach numbers and lift coefficients.

The aerodynamic effect of modifying the wing inboard trailing-edge camber of the model with the contoured body, horizontal tail ($i_t = -1^\circ$), and vertical tail is shown in the basic-data plots of figure 10 and the summary-data plots of figure 11. The lift data of figure 10(a) show that the angle of zero lift was shifted about 1° in the positive direction at all Mach numbers for the model with the modified wing trailing edge. The drag polars of figure 10(b) show a lower value of drag coefficient near zero lift coefficient for the model with the modified wing trailing edge than for the model with the original trailing edge. The modified configuration, however, had higher drag coefficients at lift coefficients in the region of maximum lift-drag ratio and had lower values of maximum lift-drag ratio (fig. 11(a)). The pitching-moment data of figure 10(c) show that the wing trailing-edge modification caused a downward displacement of the pitching-moment curves at all Mach numbers. Figure 10(c) also shows that pitch-up, which was encountered by the model with the original wing trailing edge at a lift coefficient of about 0.45 at Mach numbers of 0.92, 0.94, and 0.96, was not present at those Mach numbers for the model with the modified wing trailing edge.

Summary plots showing the effect of the modified wing trailing edge on the lift coefficient for maximum lift-drag ratio, the maximum lift-drag ratio, and the drag coefficient at lift coefficients of 0.2 and 0.4 are presented in figure 11(a). Some additional summary data are presented in figure 11(b) for the two model configurations at zero angle of attack. This figure shows that the wing trailing-edge modification caused a reduction in the model lift and pitching-moment coefficients at zero angle of attack at all Mach numbers below 0.96.

The basic longitudinal aerodynamic characteristics of the model with the contoured body, modified wing trailing edge, horizontal tail ($i_t = 2^\circ$), and vertical tail are presented in figure 12. Horizontal-tail effectiveness was determined from the data of figure 12 ($i_t = 2^\circ$) and figure 8 ($i_t = -1^\circ$) at lift coefficients of 0.2, 0.4, and 0.6. (See fig. 13.) A gradual increase in tail effectiveness with Mach number occurred at all three lift coefficients up to a Mach number of about 0.93 where the largest value of tail effectiveness was obtained.

The basic longitudinal aerodynamic characteristics of the model without horizontal and vertical tails are presented in figure 14 for the contoured body configuration and in figure 15 for the cylindrical and modified cylindrical configurations. The variation with Mach number of the summary aerodynamic characteristics for the three body-wing configurations is presented in figure 16. The data of figure 16(a) show that the contoured body configuration had higher maximum lift-drag ratios than the other two configurations at Mach numbers above 0.84. The static longitudinal stability parameter $C_{m_{CL}}$, shown in figure 16(b), was nearly constant with Mach number for all three body configurations up to a Mach number of about 0.86 where an increase in stability began for the cylindrical and modified cylindrical body configurations.

The cylindrical body was tested alone. The basic drag-coefficient and pitching-moment-coefficient data plotted against angle of attack for this configuration are presented in figure 17.

CONCLUSIONS

The longitudinal aerodynamic characteristics of a model with a modified wing trailing edge were determined at Mach numbers from 0.40 to 0.96. The modification consisted of a reduction in the effective camber of the inboard wing sections near the trailing edge to reduce shock-induced flow separation on the wing upper surface at high subsonic speeds. An analysis of the test results has led to the following conclusions:

1. The modified wing trailing edge generally reduced the drag coefficient at low lift coefficients but increased the drag coefficient in the range of lift coefficients for maximum lift-drag ratio and resulted in lower values of maximum lift-drag ratio.

2. The wing trailing-edge modification alleviated model pitch-up which was encountered by the model with the original wing trailing edge at a lift coefficient of about 0.45 at Mach numbers of 0.92, 0.94, and 0.96.

3. The modified wing trailing edge caused an increase of about 1° in the angle of zero lift of the model at all Mach numbers and a decrease in the model pitching-moment coefficient at zero angle of attack at all Mach numbers below 0.96.

4. The effect of fixed transition on pitch was destabilizing at low positive lift coefficients and reduced the lift-curve slope slightly at Mach numbers from 0.84 to 0.96.

Langley Research Center,
National Aeronautics and Space Administration,
Langley Station, Hampton, Va., March 25, 1963.

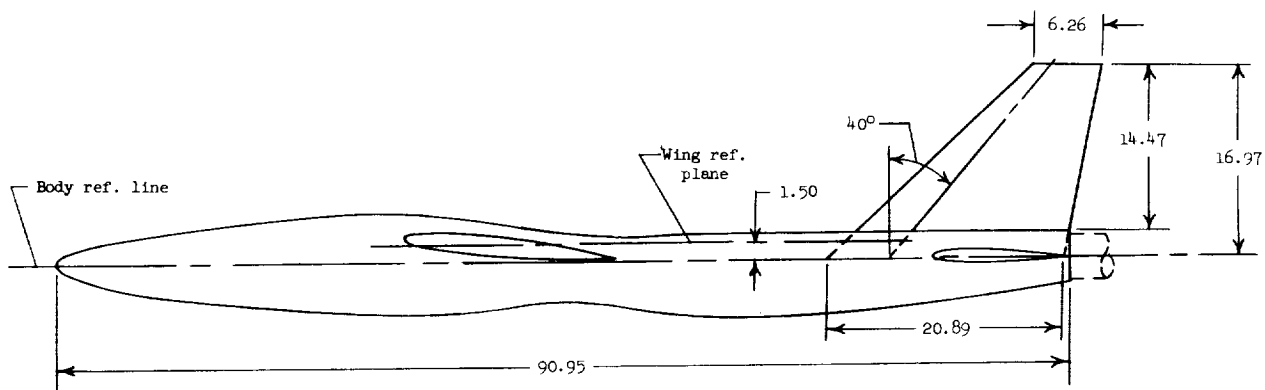
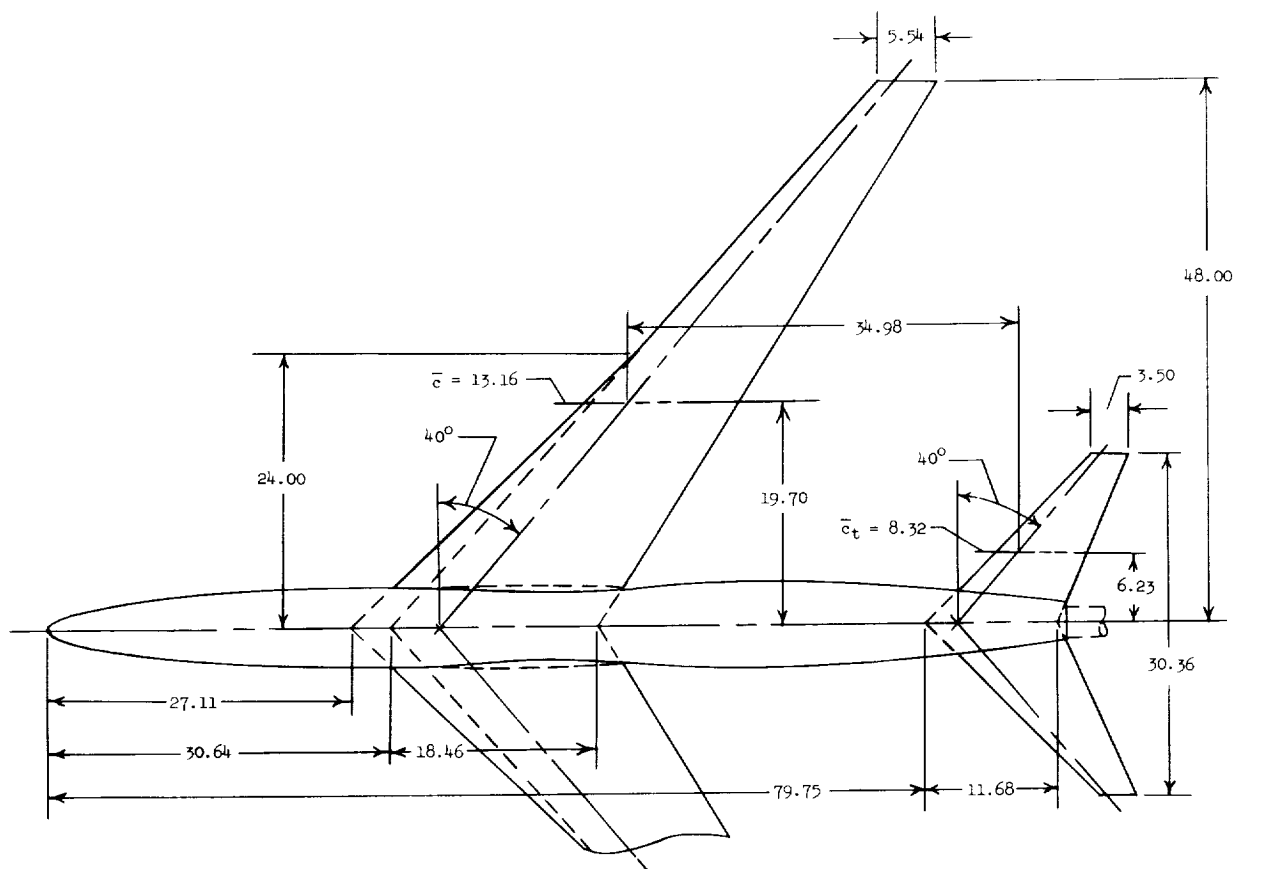
REFERENCES

1. Heath, Atwood R., Jr.: Longitudinal Aerodynamic Characteristics of a High-Subsonic-Speed Transport Airplane Model With A Cambered 40° Sweptback Wing of Aspect Ratio 8 at Mach Numbers to 0.96. NASA TN D-218, 1960.
2. Loving, Donald L.: A Wind-Tunnel Investigation of a Transonic-Transport Configuration Utilizing Drag-Reducing Devices at Mach Numbers From 0.20 to 1.03. NASA TN D-636, 1961.
3. Whitcomb, Richard T., and Heath, Atwood R., Jr.: Several Methods for Reducing the Drag of Transport Configurations at High Subsonic Speeds. NASA MEMO 2-25-59L, 1959.
4. Whitcomb, Richard T.: Special Bodies Added on a Wing To Reduce Shock-Induced Boundary-Layer Separation at High Subsonic Speeds. NACA TN 4293, 1958.
5. Whitcomb, Richard T.: A Fuselage Addition To Increase Drag-Rise Mach Number of Subsonic Airplanes at Lifting Conditions. NACA TN 4290, 1958.



L-62-1273

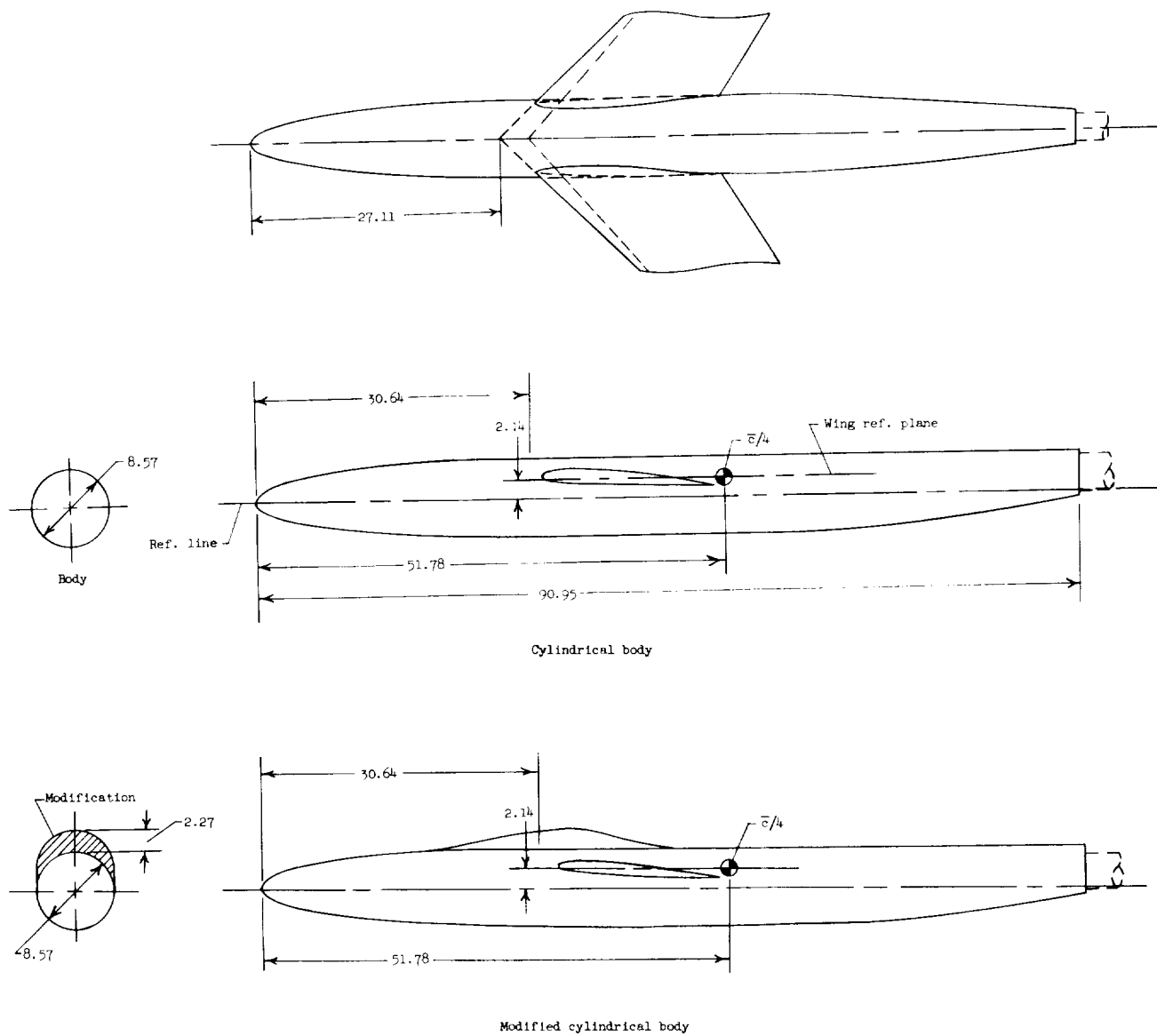
Figure 1.- Photograph showing model with contoured body and without tail surfaces mounted in Langley 16-foot transonic tunnel.



Model station 0

(a) Contoured body, wing, and horizontal and vertical tails.

Figure 2.- Sketches of model illustrating wing, bodies, and tail surfaces. (All dimensions in inches unless otherwise indicated.)



(b) Cylindrical and modified cylindrical bodies.

Figure 2.- Concluded.

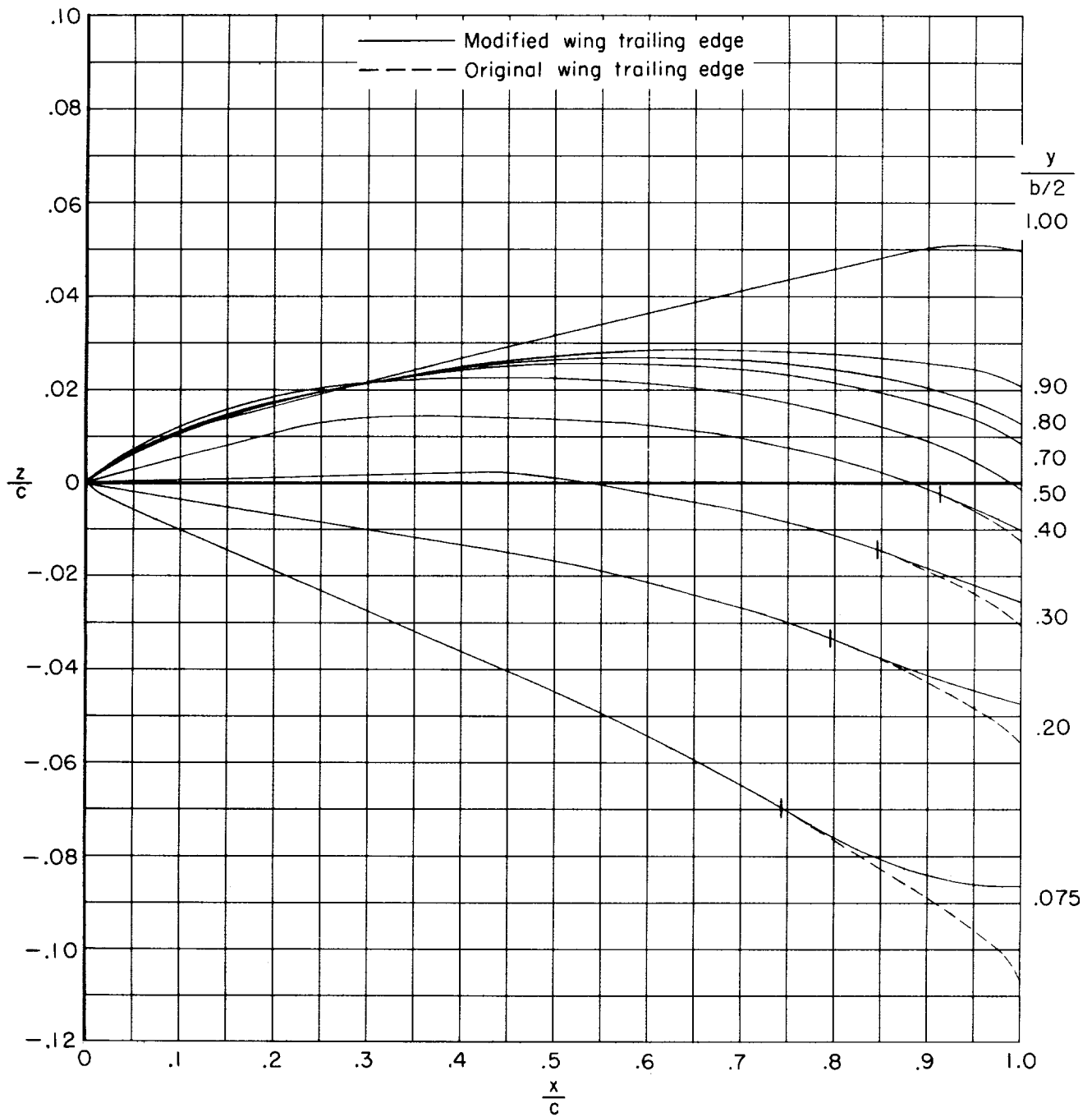


Figure 3.- Nondimensionalized wing camber lines for wing with and without the trailing-edge camber modification. Tick marks indicate local chord stations at which camber modification starts.

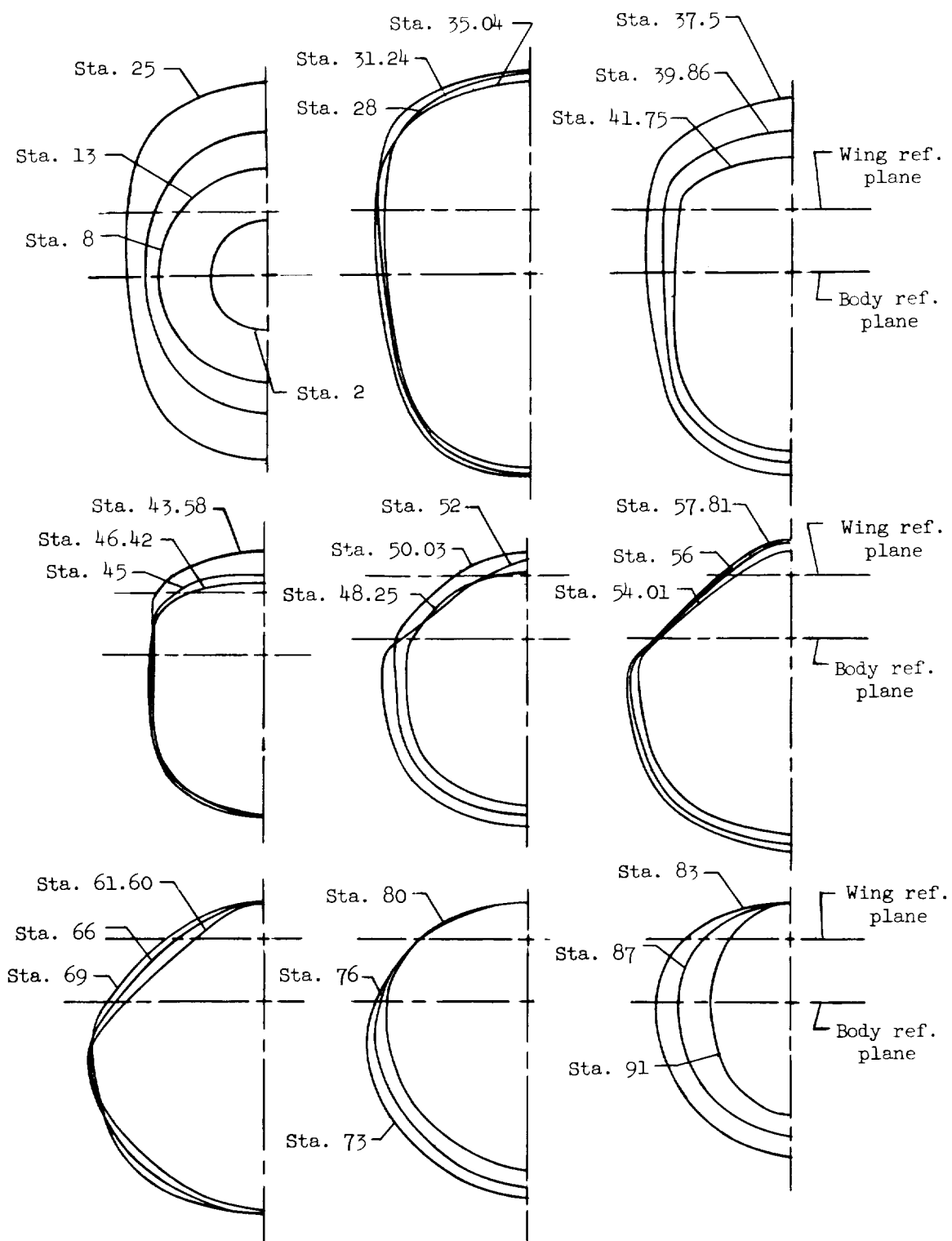


Figure 4.- Cross sections of contoured body. (Model stations in inches.)

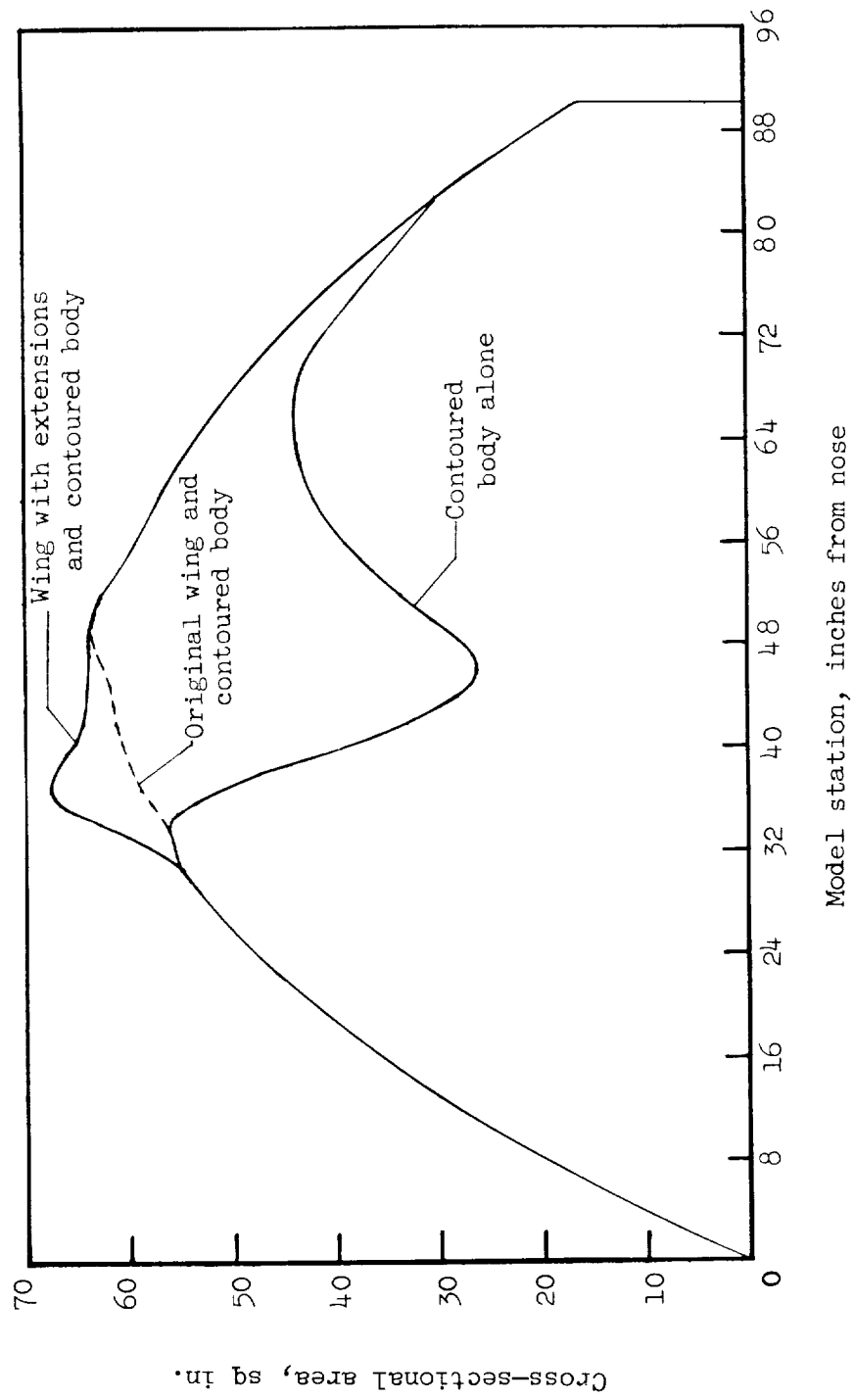


Figure 5.- Cross-sectional area distribution for wing with contoured body.

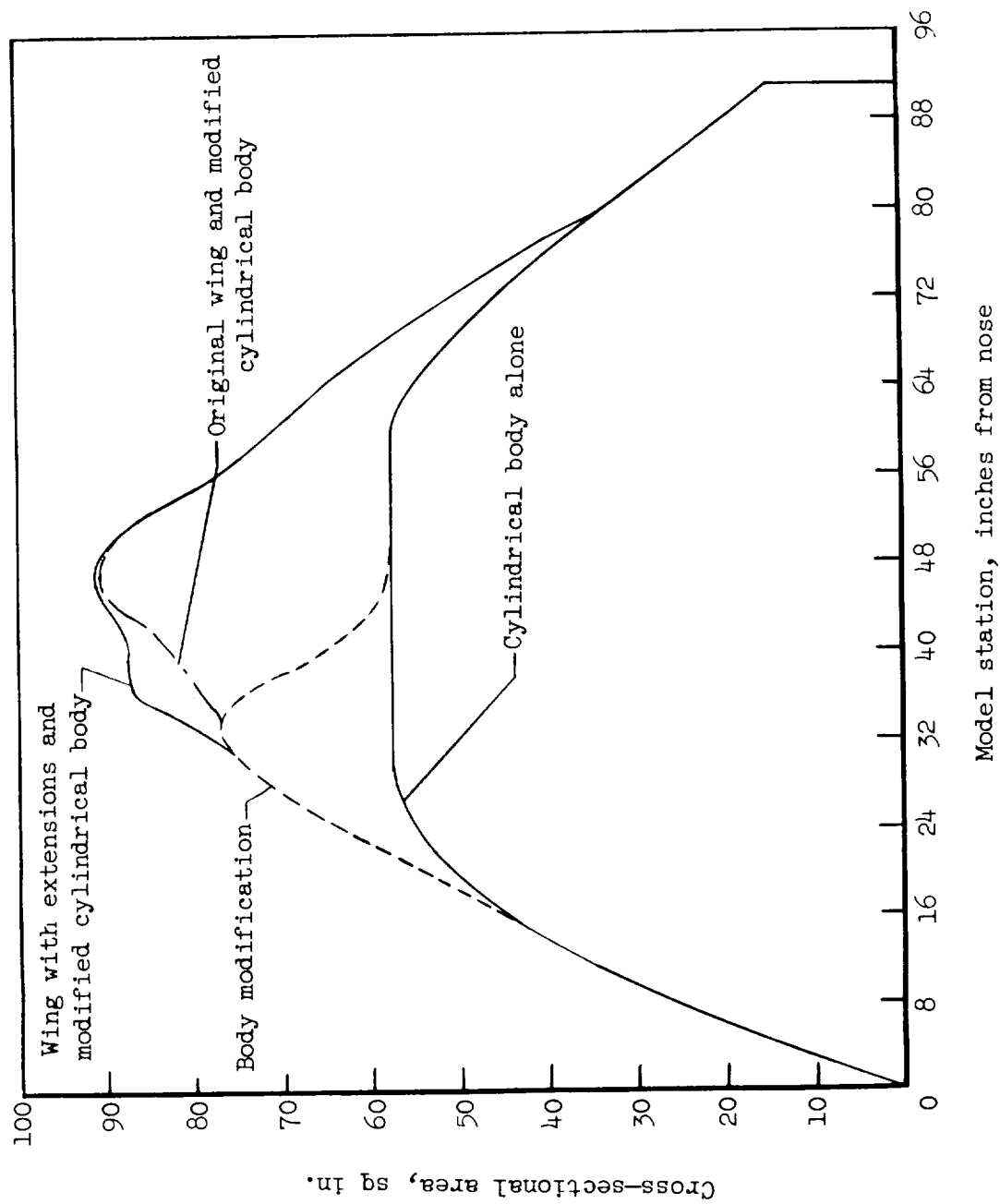
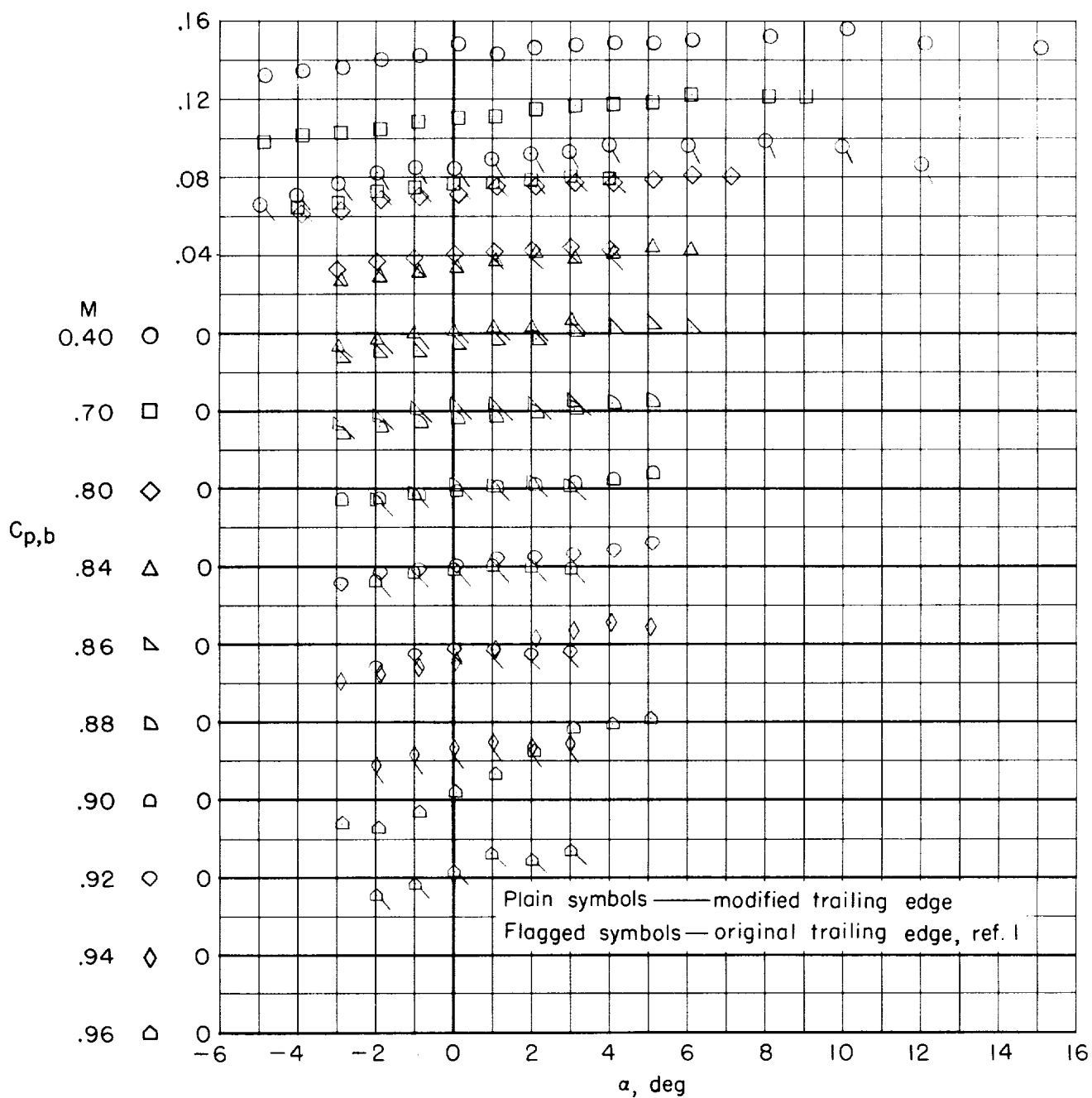
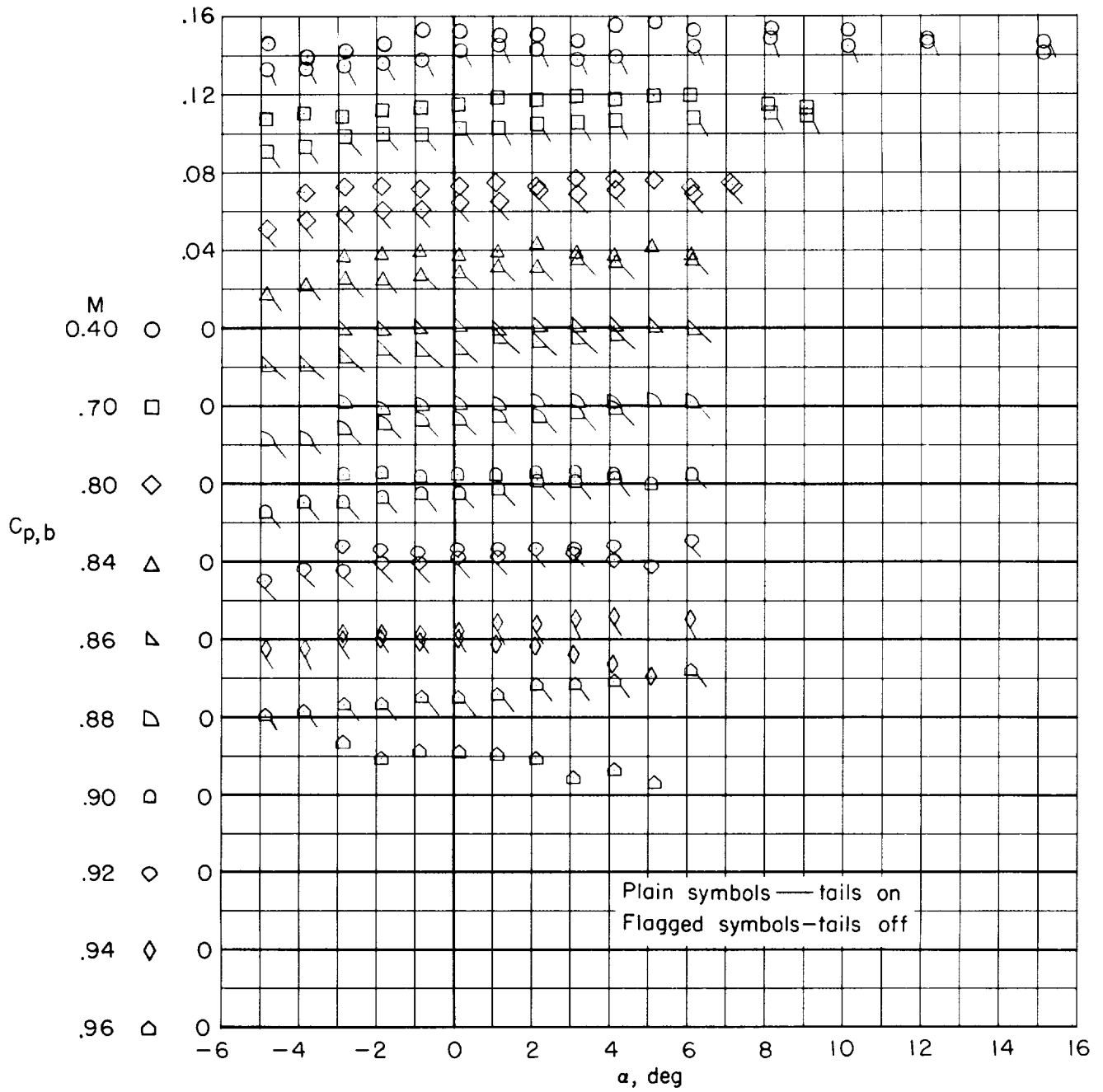


Figure 6.- Cross-sectional area distributions for wing with modified cylindrical bodies.



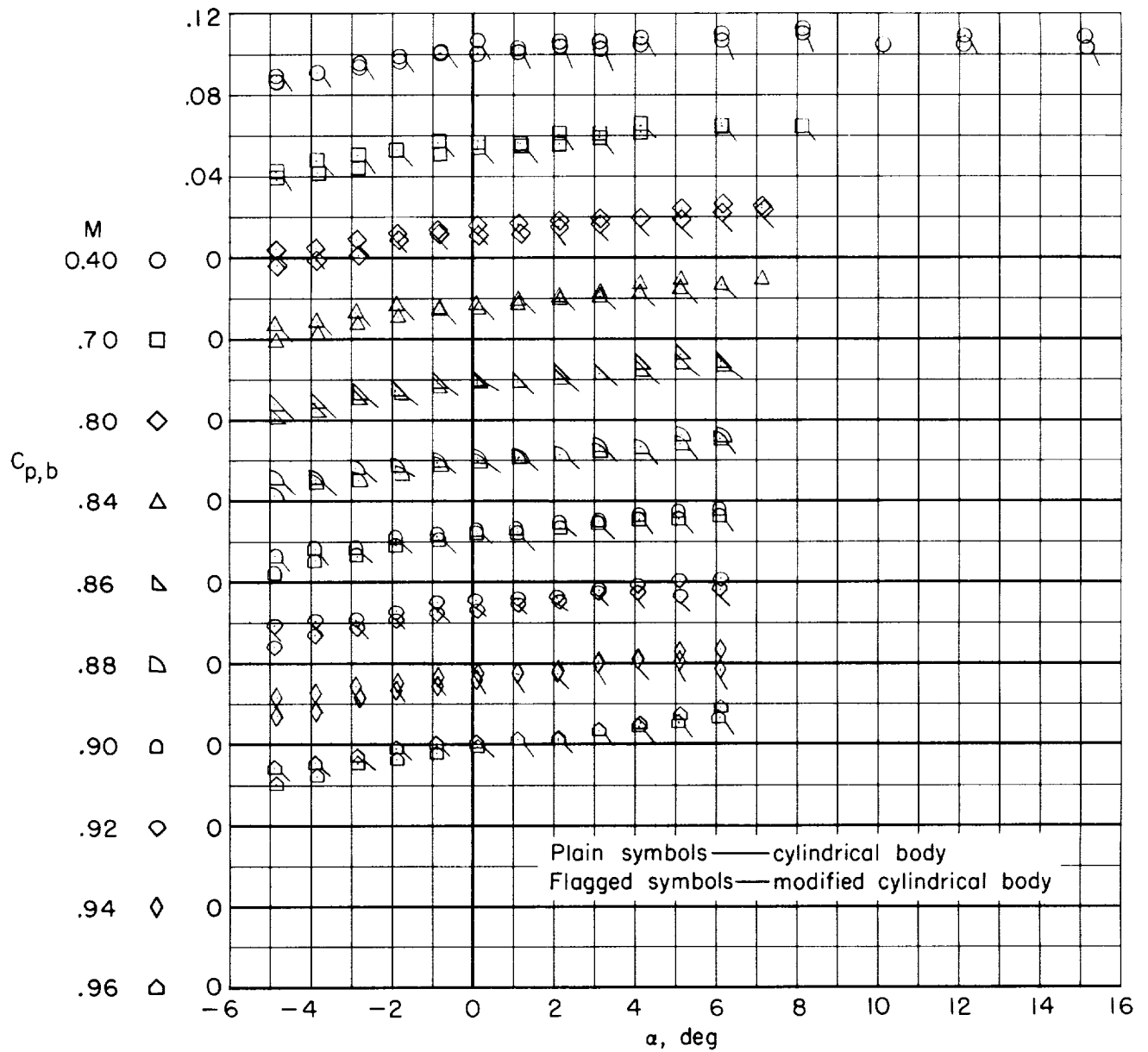
(a) Contoured body, wing with and without modified trailing edge, vertical tail, and horizontal tail ($i_t = -1^\circ$).

Figure 7.- Base pressure coefficients against angle of attack for various model configurations.



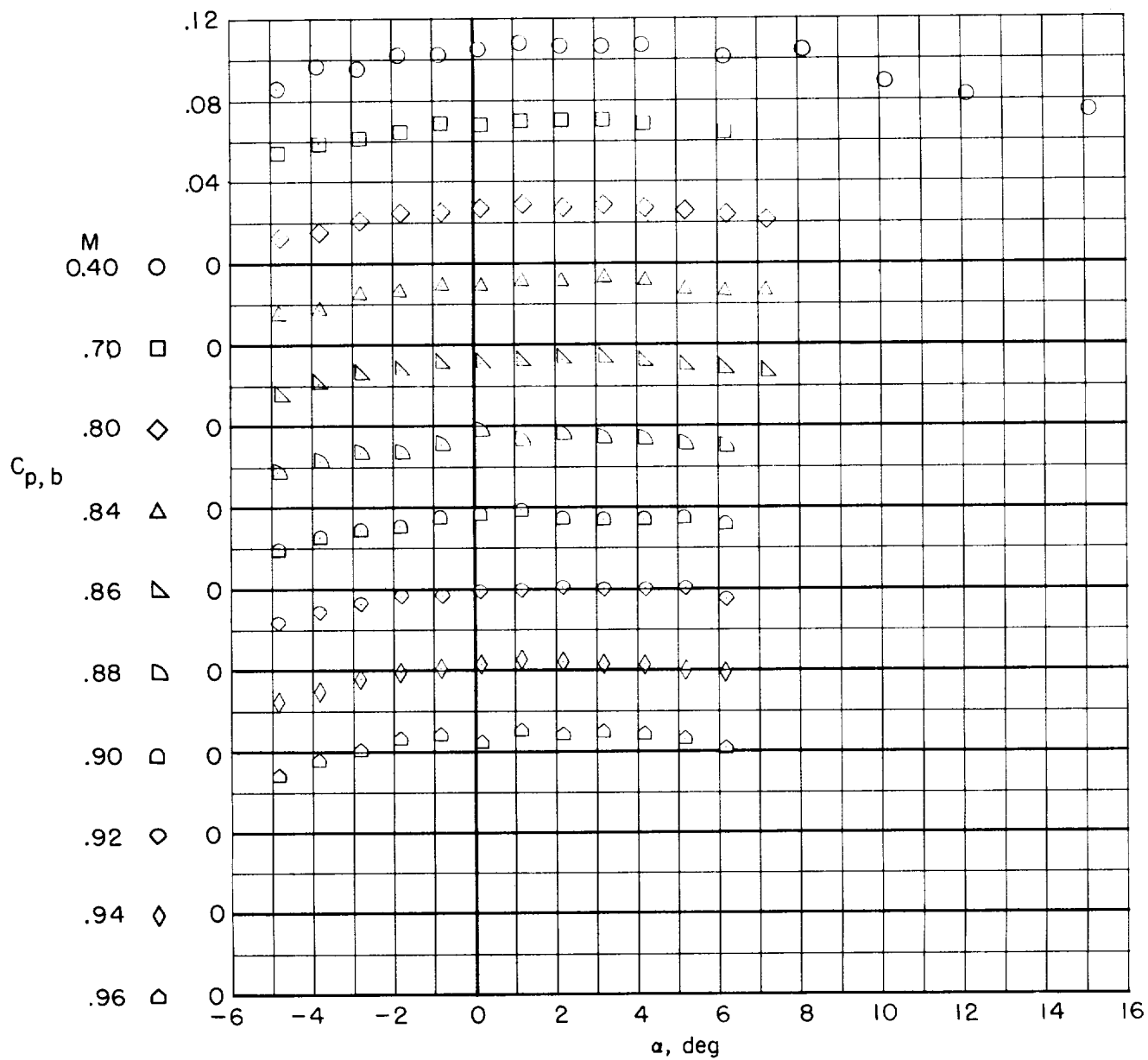
(b) Contoured body and wing with modified trailing edge with vertical and horizontal tails ($i_t = 2^\circ$) on and off.

Figure 7.- Continued.



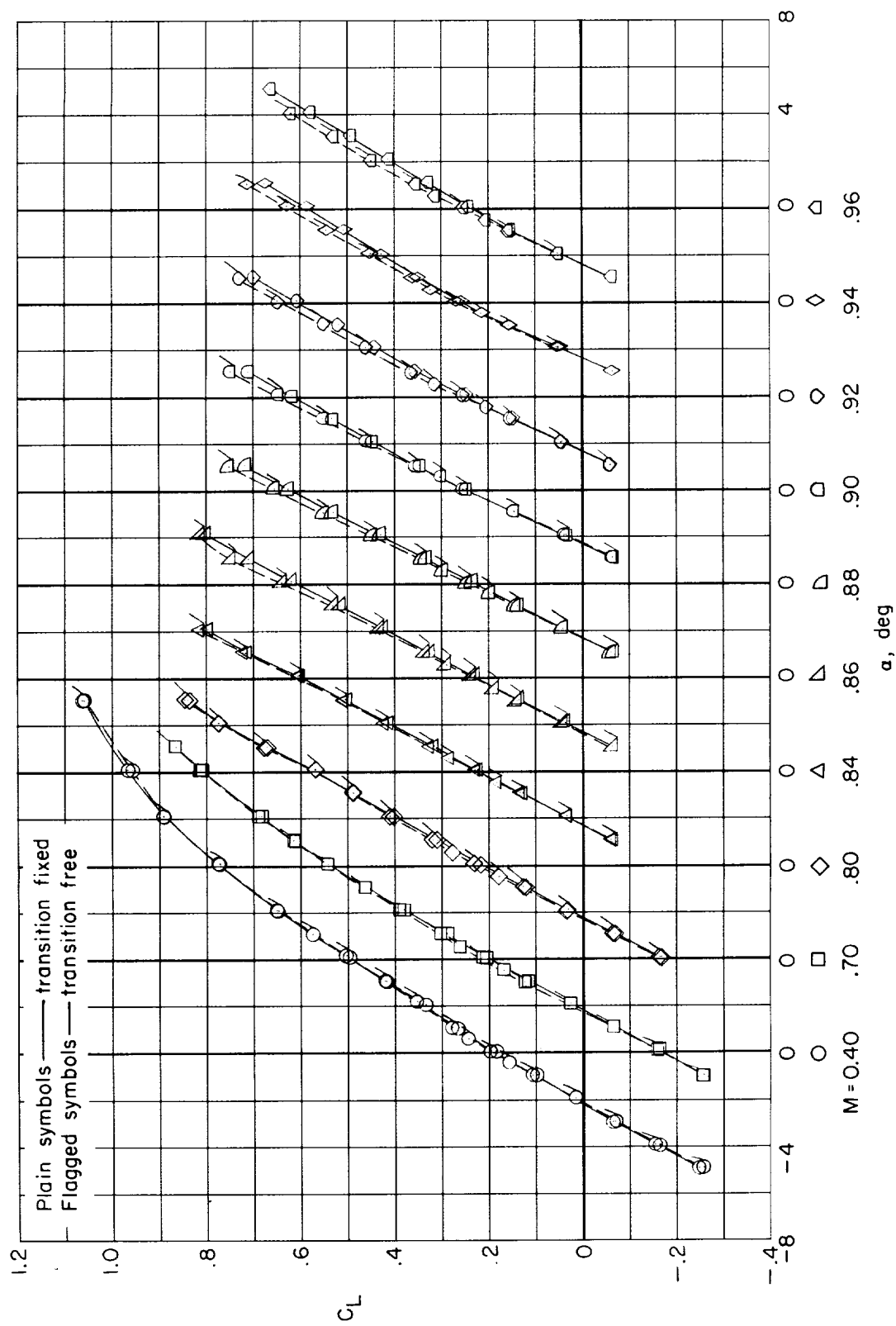
(c) Cylindrical and modified cylindrical bodies and wing with modified trailing edge.

Figure 7.- Continued.



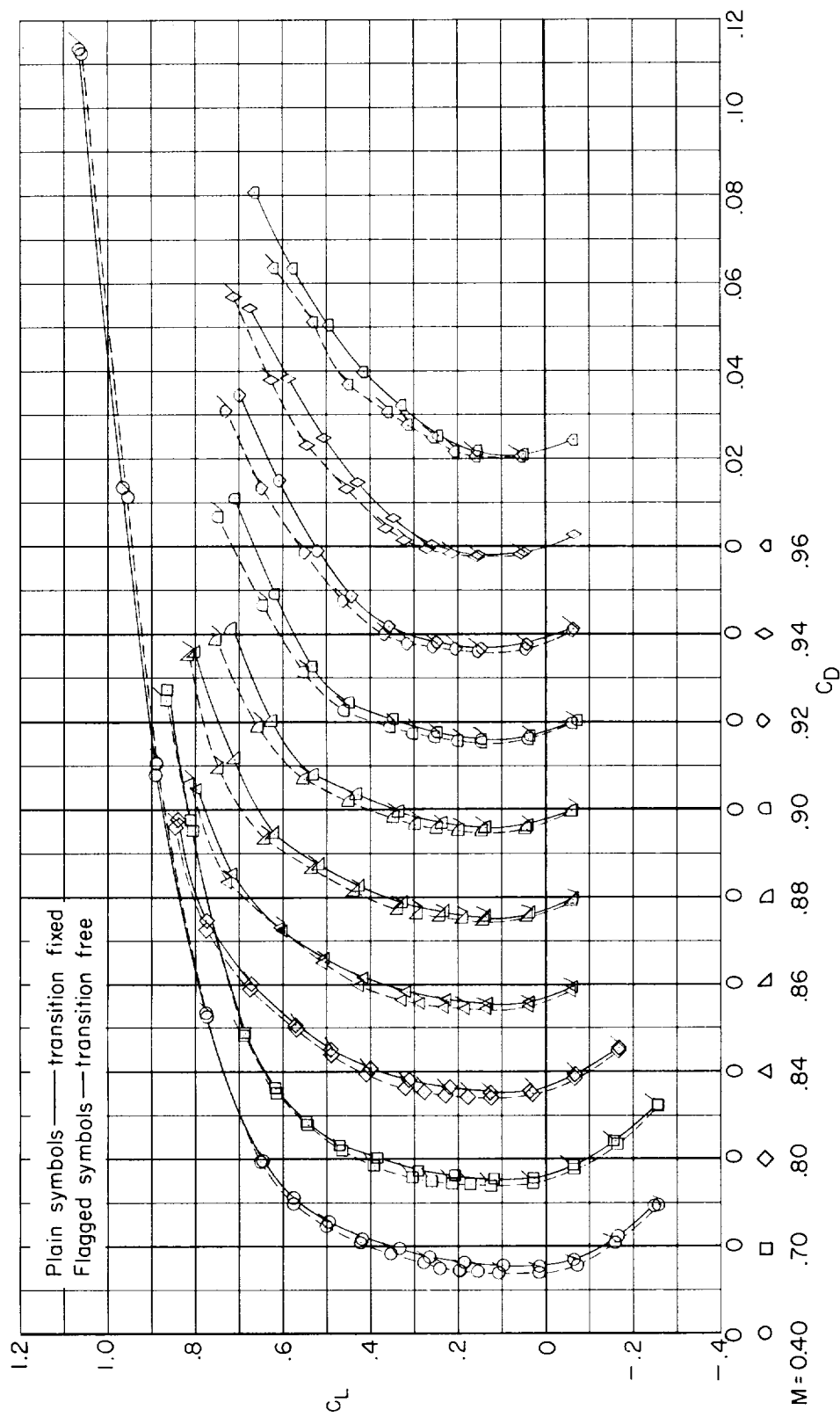
(d) Cylindrical body alone.

Figure 7.- Concluded.



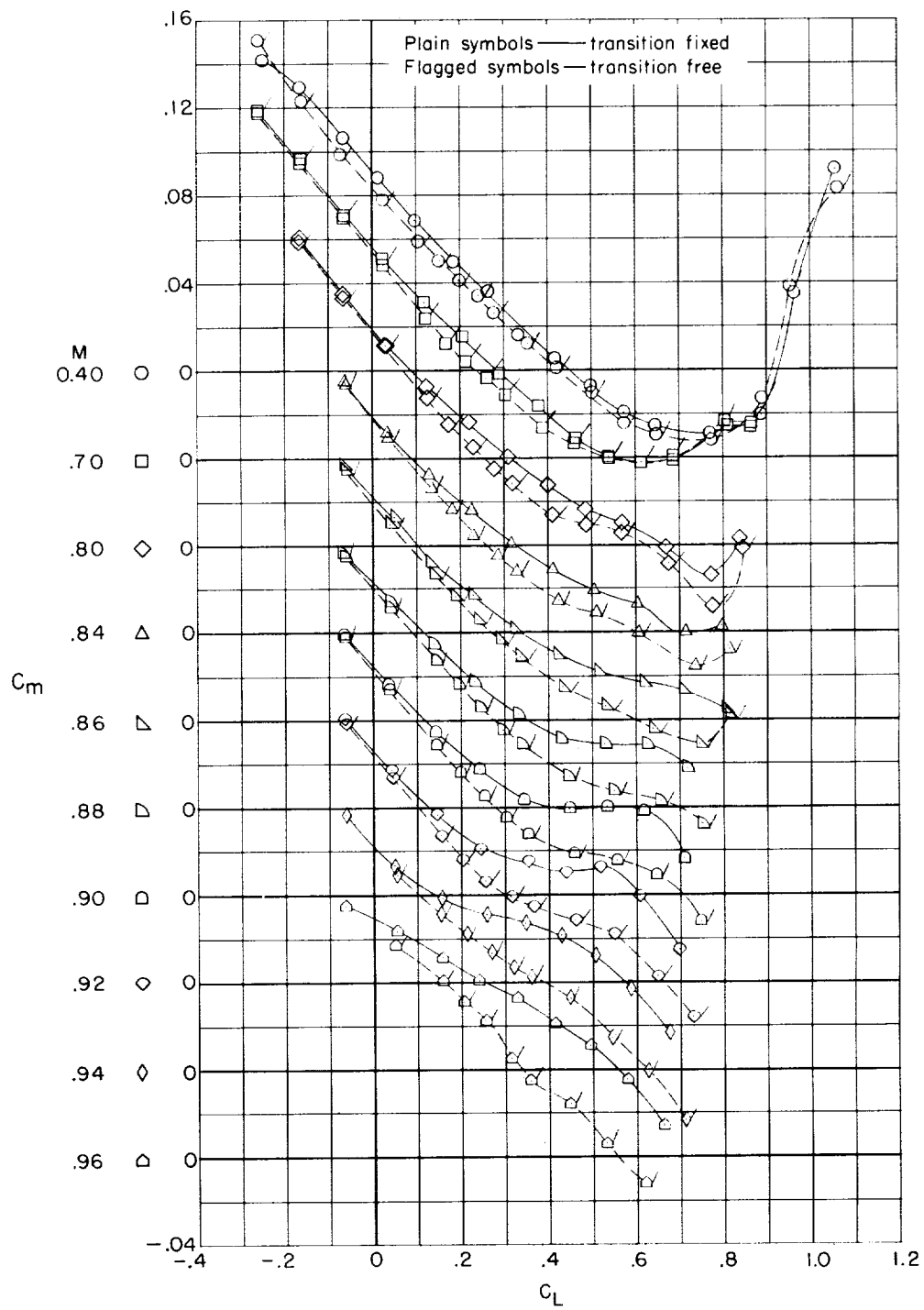
(a) Lift coefficient.

Figure 8.- Effect of fixed transition on longitudinal aerodynamic characteristics of model with contoured body, wing (modified inboard trailing edge), vertical tail, and horizontal tail ($it = -1.0$).



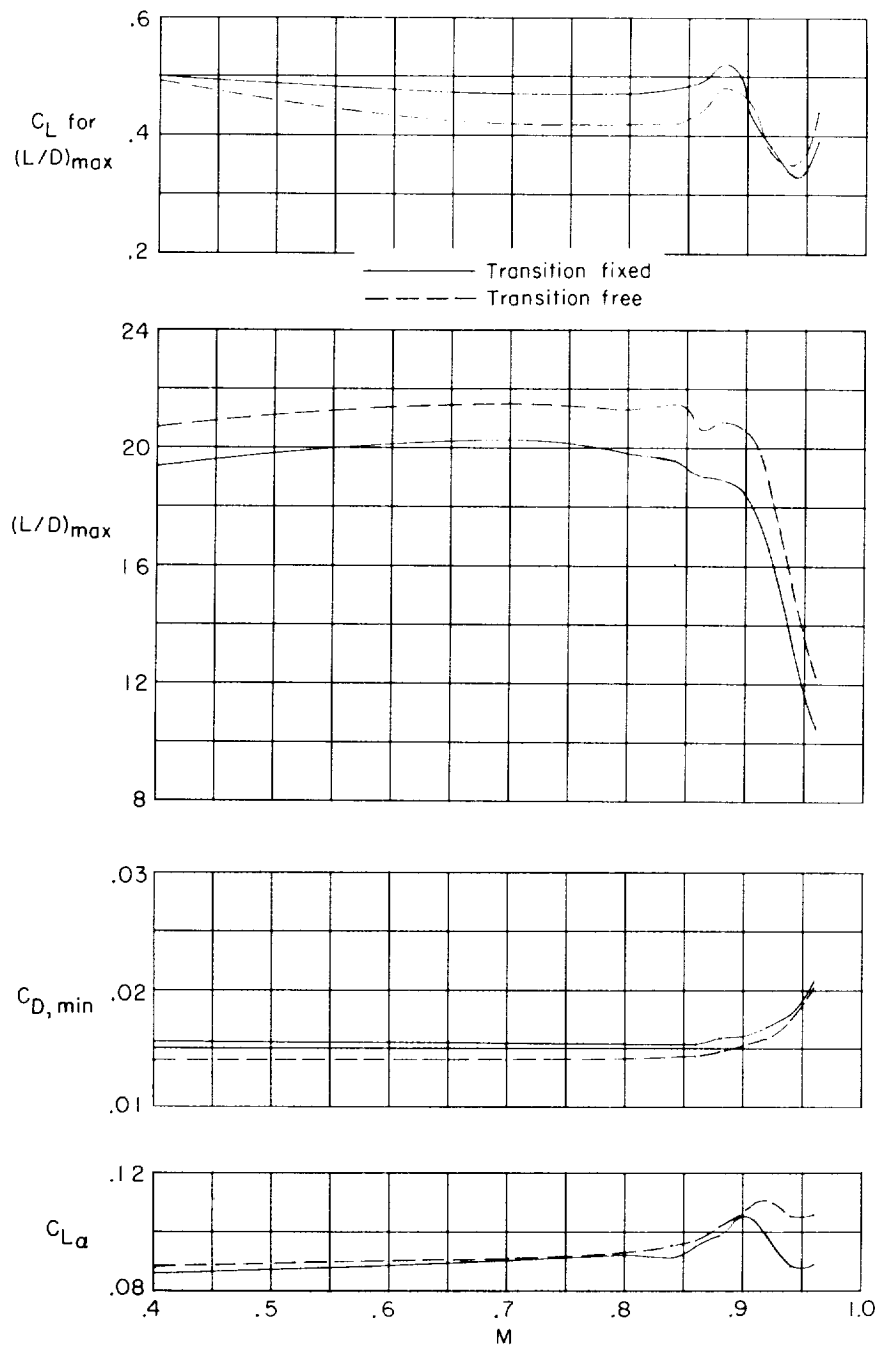
(b) Drag coefficient.

Figure 8.- Continued.



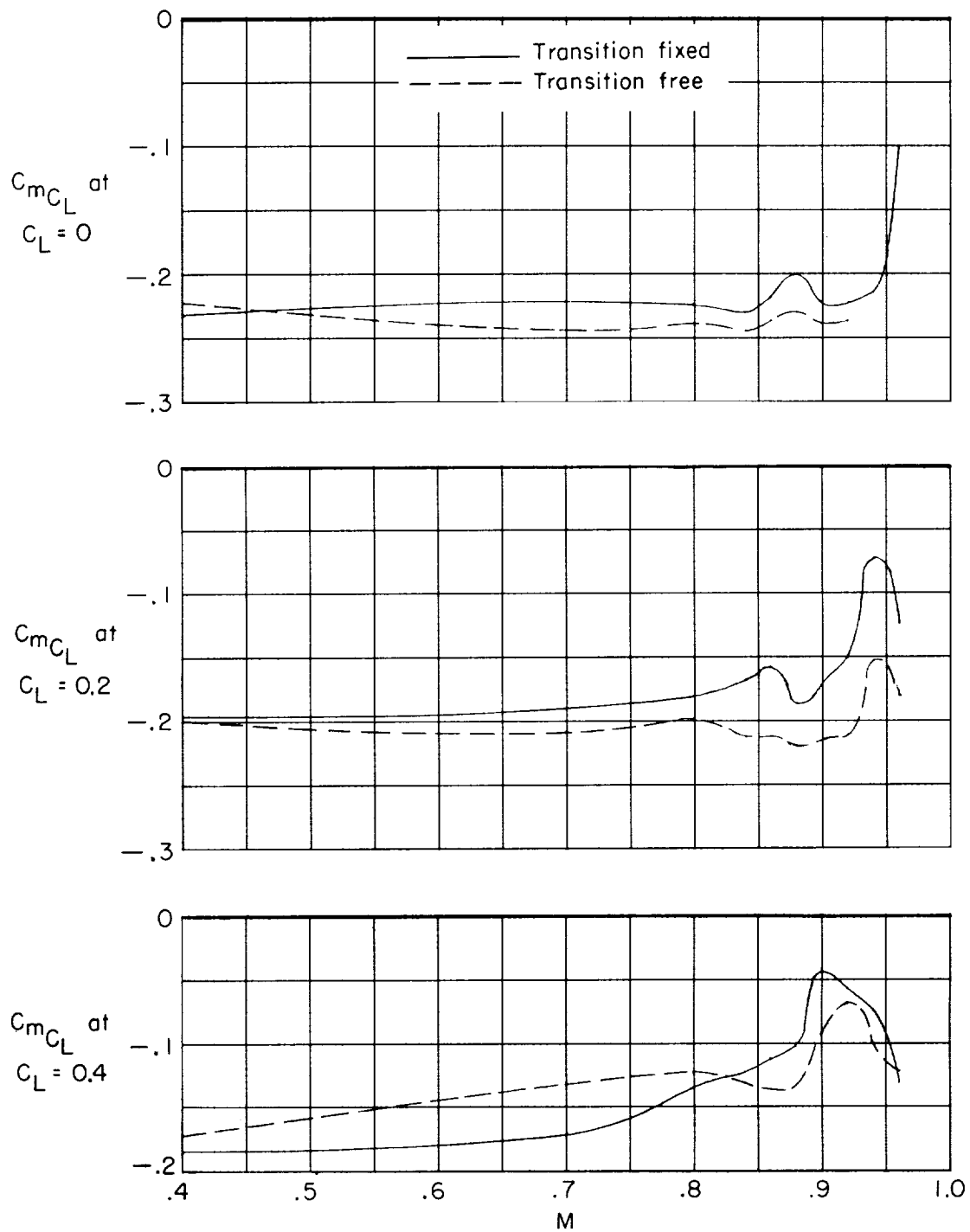
(c) Pitching-moment coefficient.

Figure 8.- Concluded.



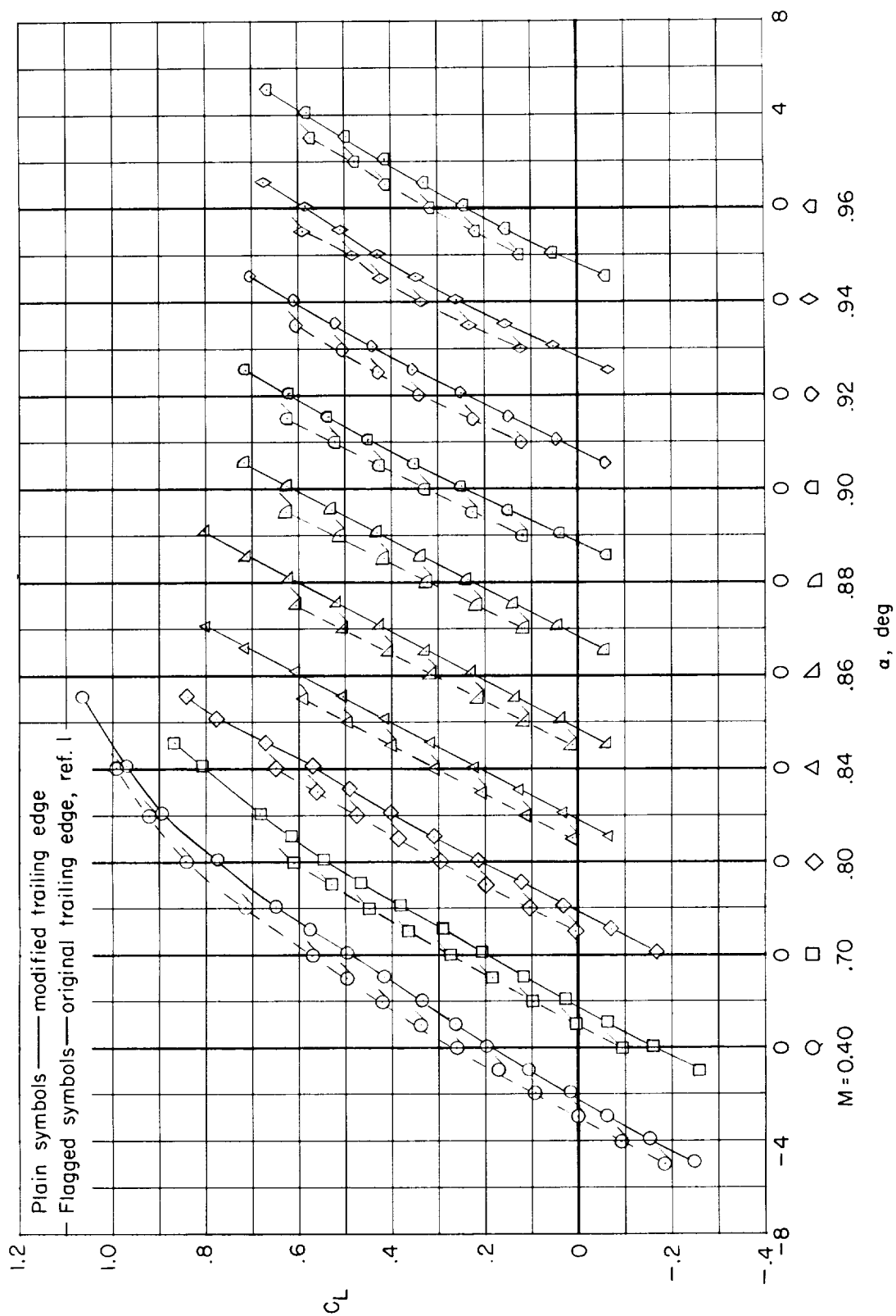
(a) C_L for $(L/D)_{\max}$; $(L/D)_{\max}$; $C_{D,min}$; $C_{L\alpha}$.

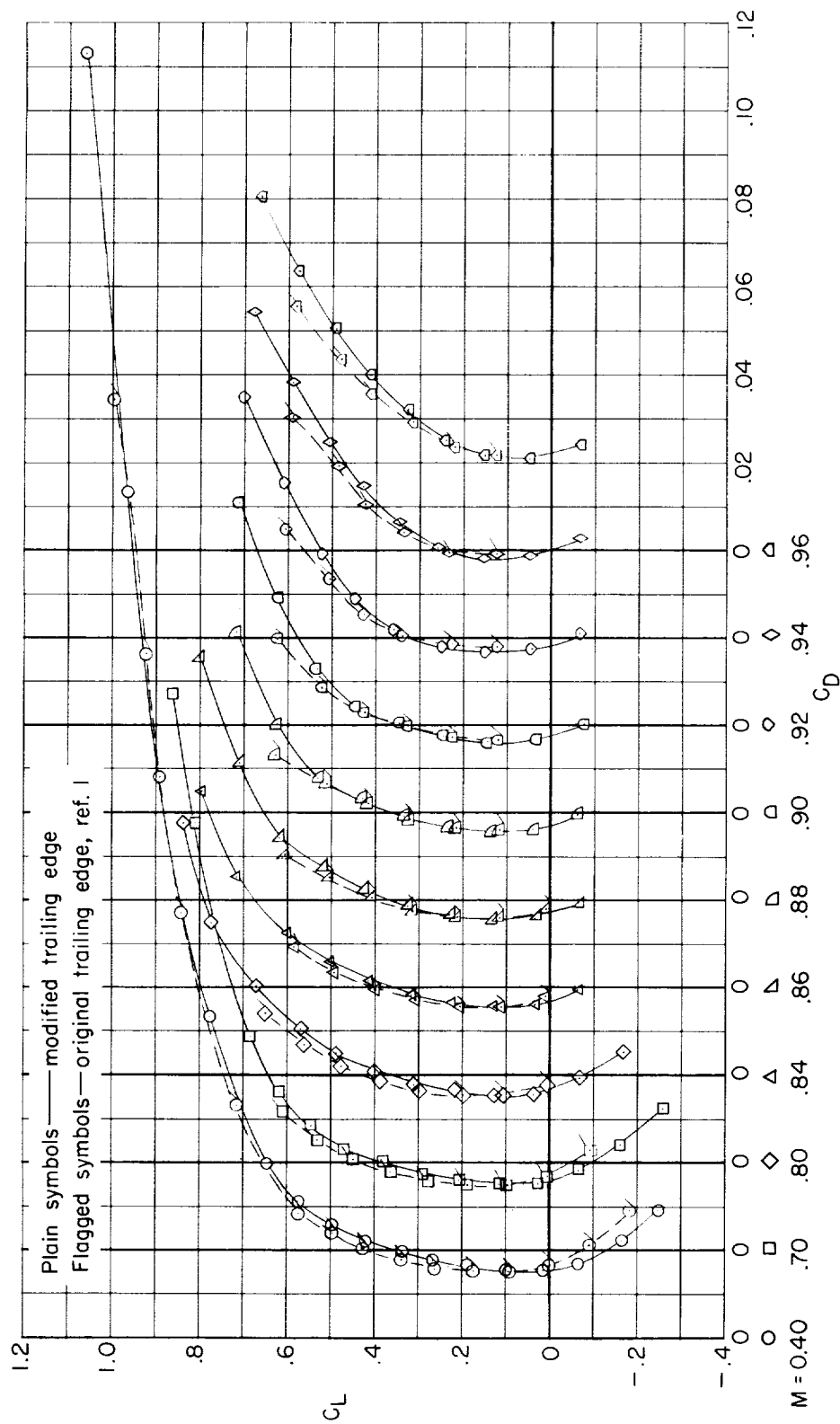
Figure 9.- Variation with Mach number of longitudinal aerodynamic characteristics of model with contoured body, wing (modified inboard trailing edge), vertical tail, and horizontal tail ($i_t = -1^\circ$) with and without fixed transition.



(b) C_{mC_L} .

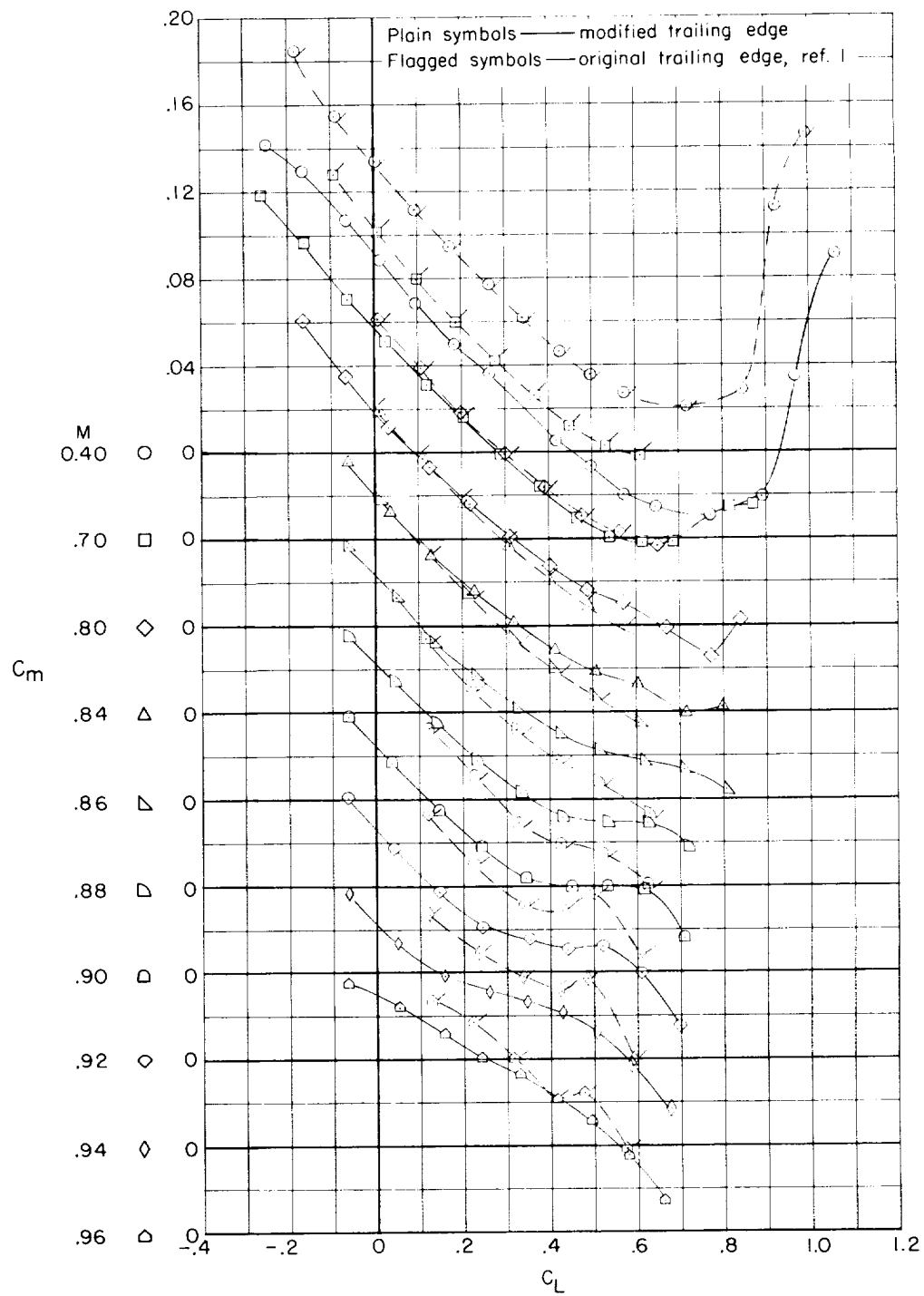
Figure 9.- Concluded.





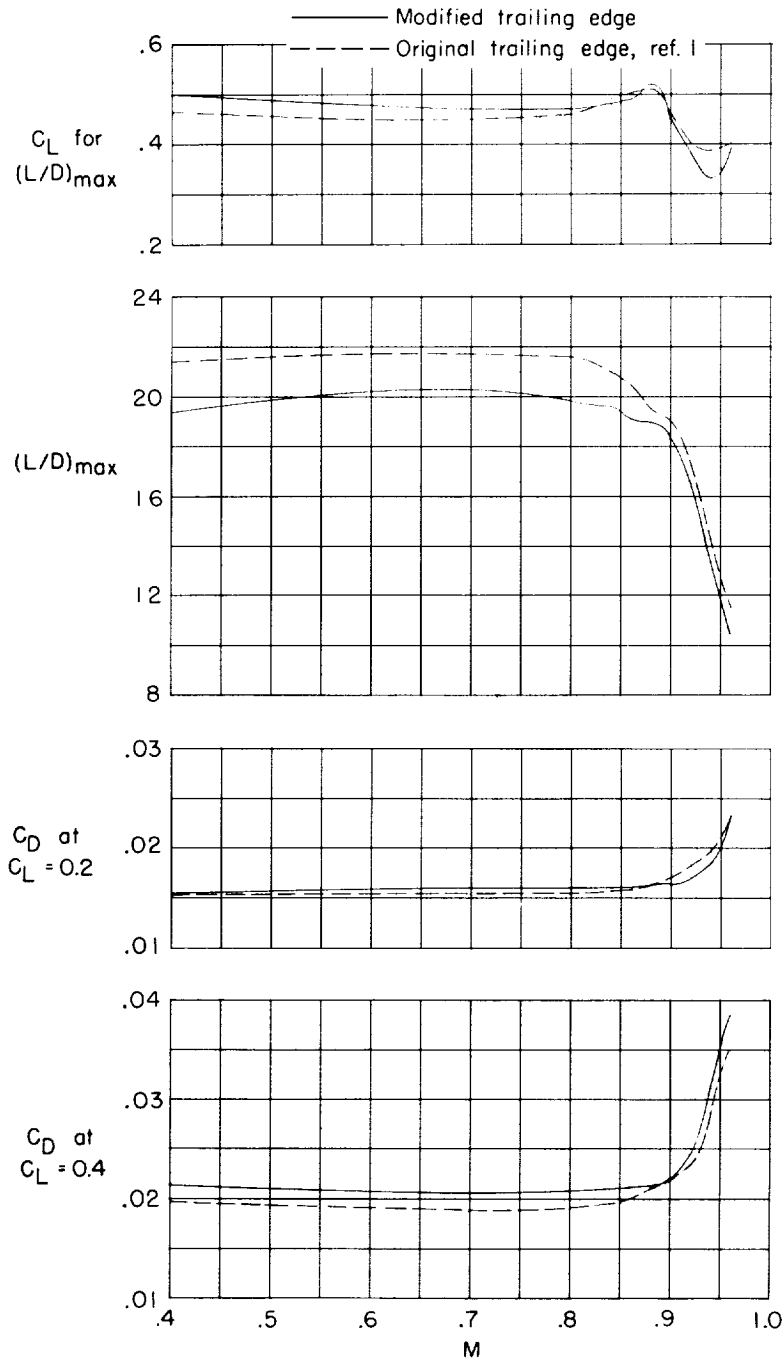
(b) Drag coefficient.

Figure 10.- Continued.



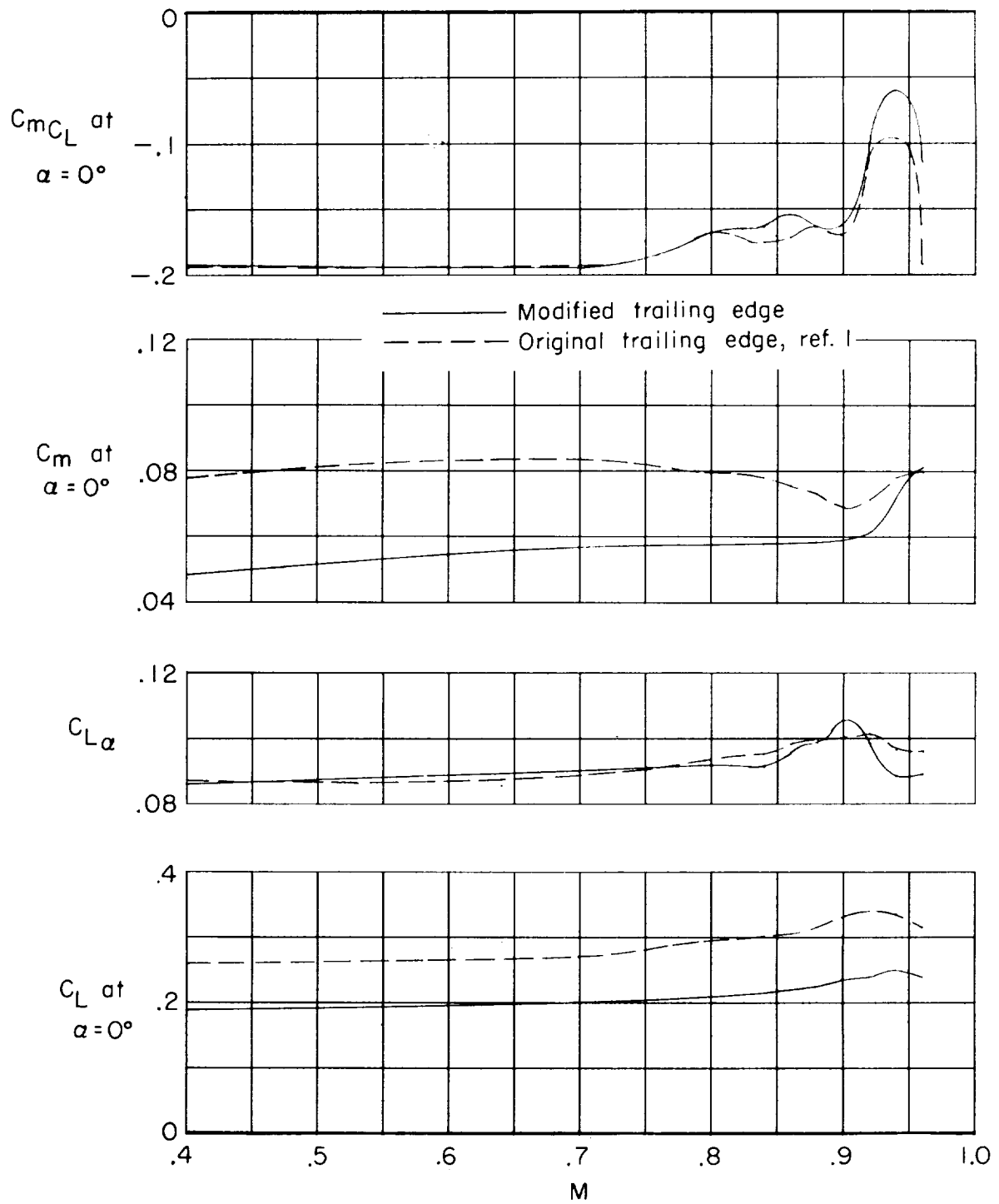
(c) Pitching-moment coefficient.

Figure 10.- Concluded.



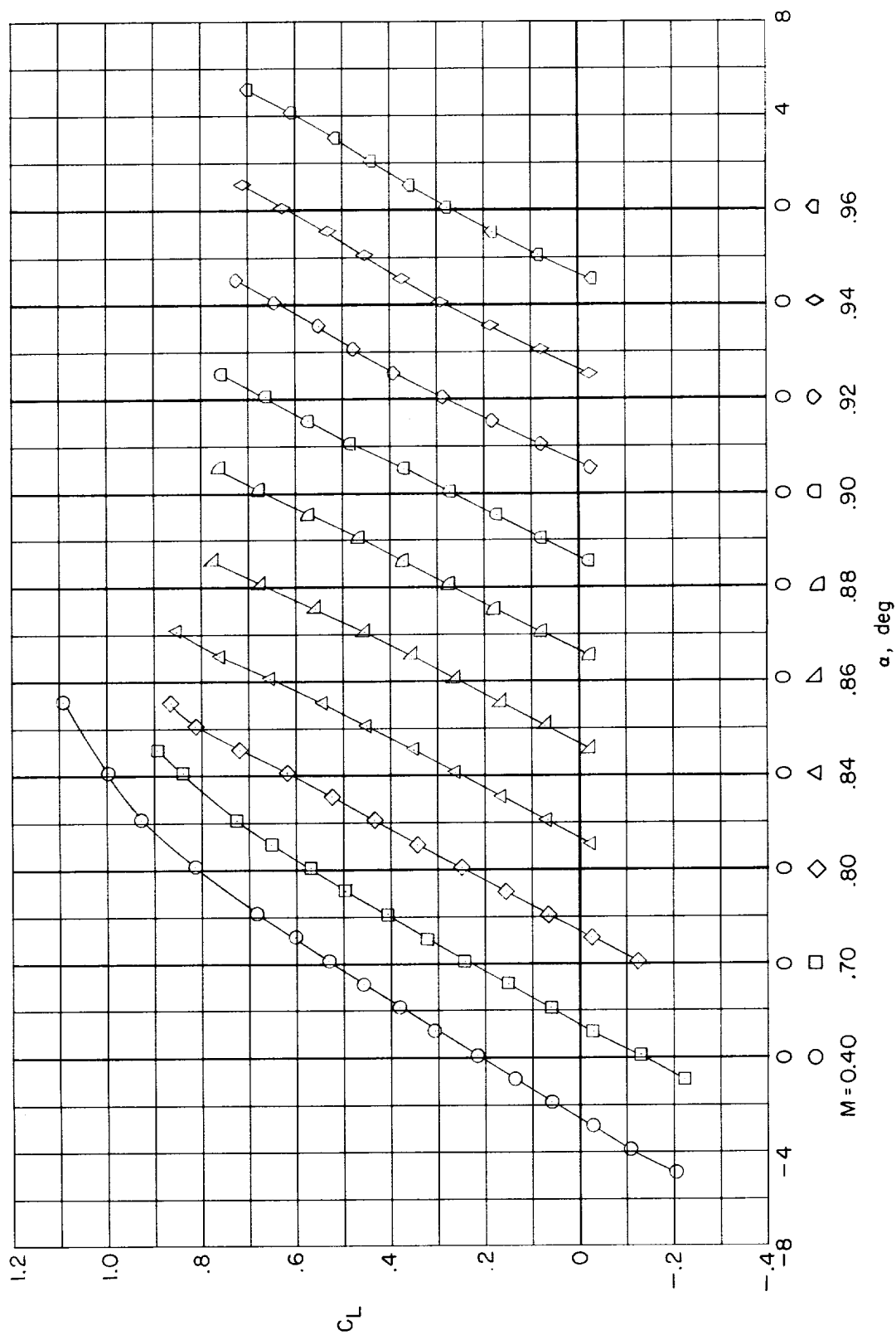
(a) C_L for $(L/D)_{\max}$; $(L/D)_{\max}$; C_D .

Figure 11.- Variation with Mach number of longitudinal aerodynamic characteristics of model with contoured body, wing with and without inboard trailing-edge modification, vertical tail, and horizontal tail ($i_t = -1^\circ$).



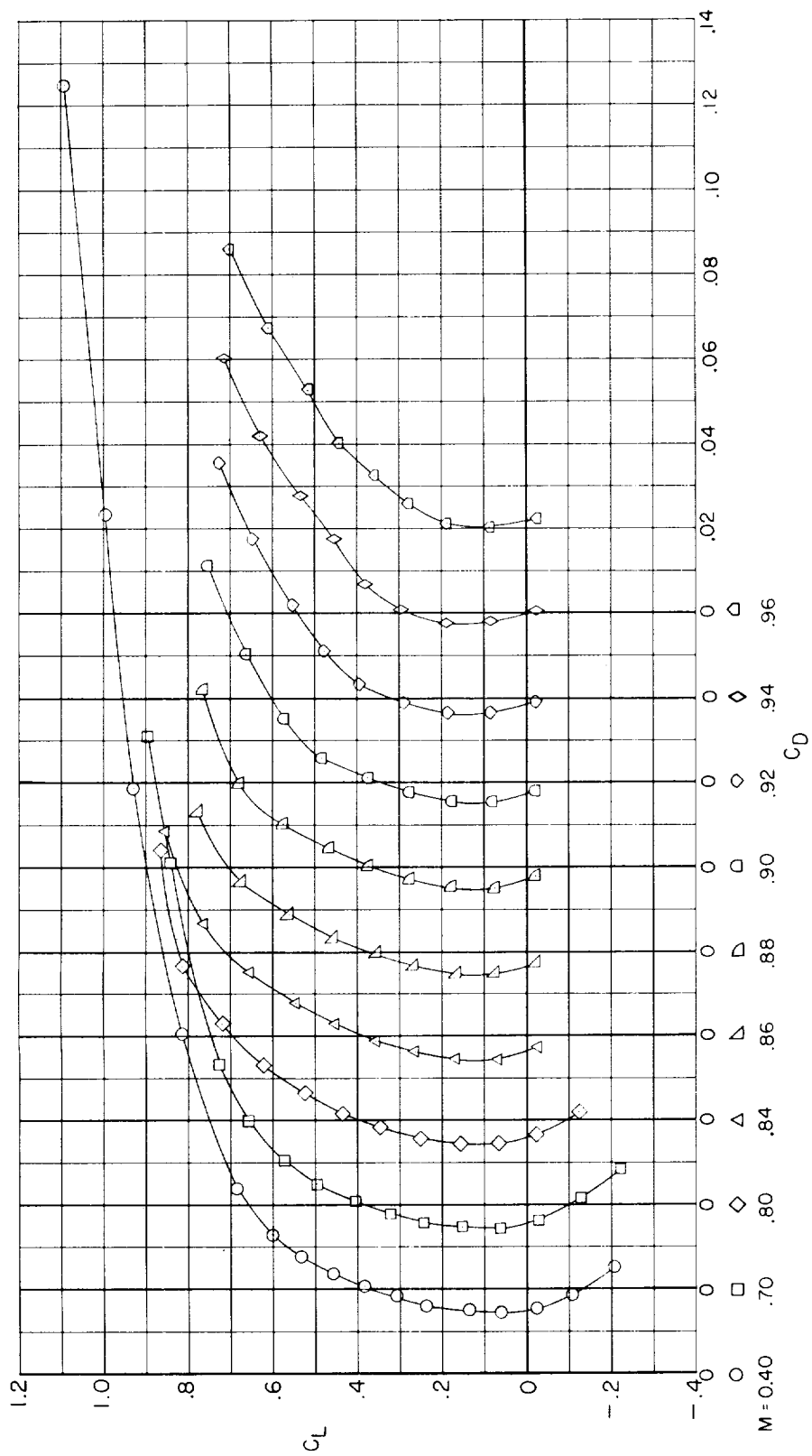
(b) C_{mC_L} at $\alpha = 0^\circ$; C_m at $\alpha = 0^\circ$; $C_{L\alpha}$; C_L at $\alpha = 0^\circ$.

Figure 11.- Concluded.



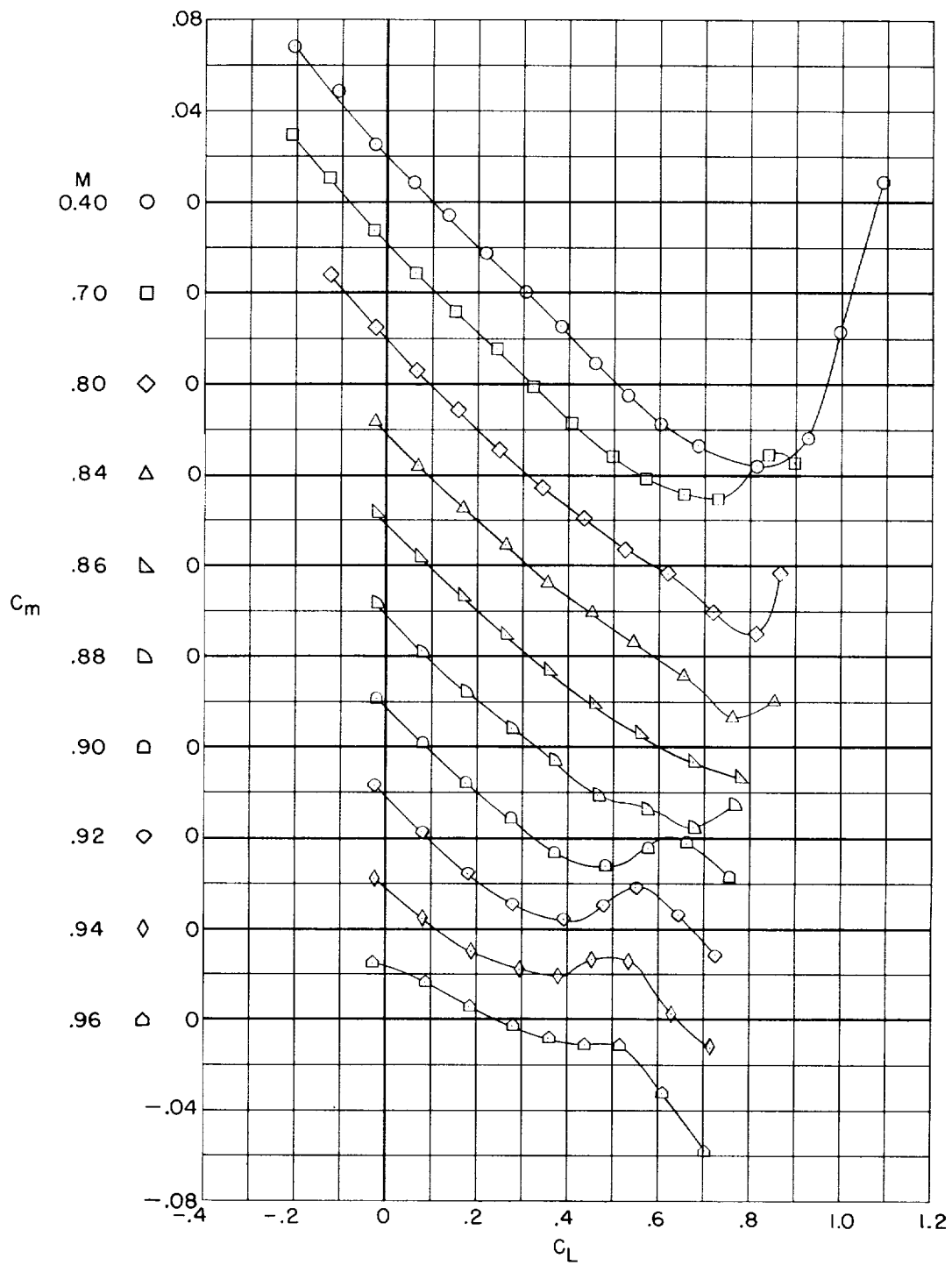
(a) Lift coefficient.

Figure 12.- Longitudinal aerodynamic characteristics of model with contoured body, wing (modified inboard trailing edge), vertical tail, and horizontal tail ($i_t = 2^\circ$).



(b) Drag coefficient.

Figure 12.- Continued.



(c) Pitching-moment coefficient.

Figure 12.- Concluded.

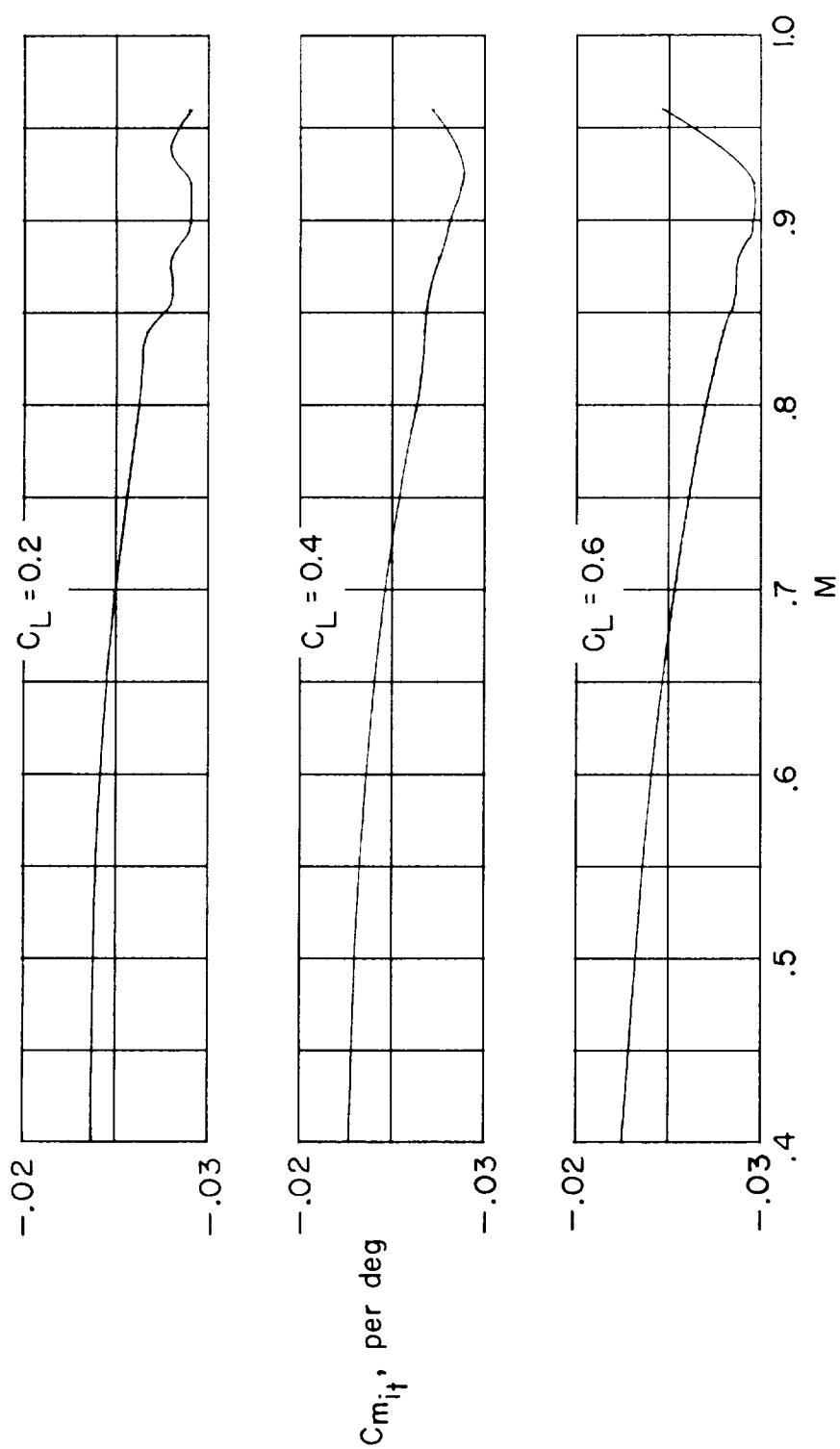
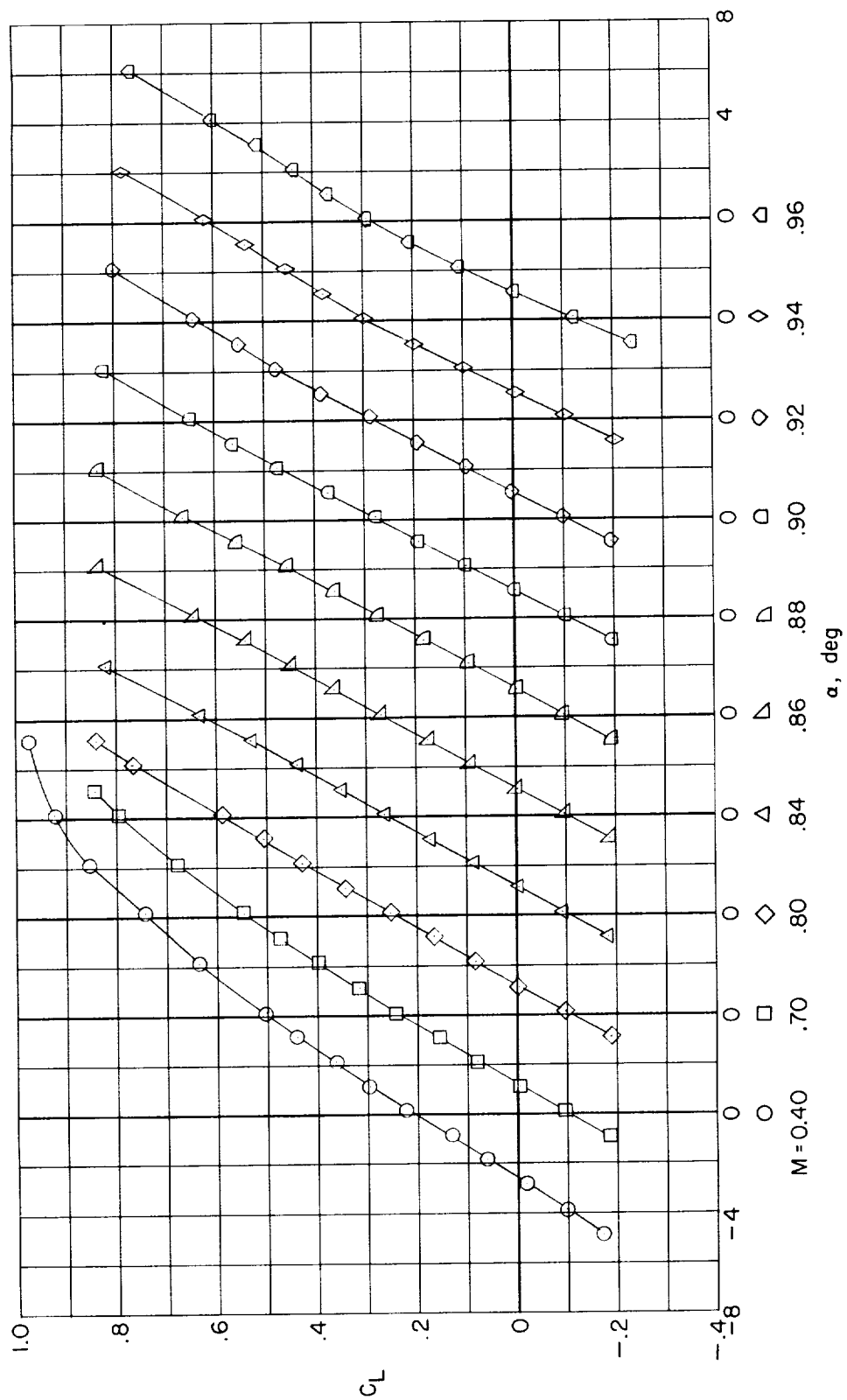
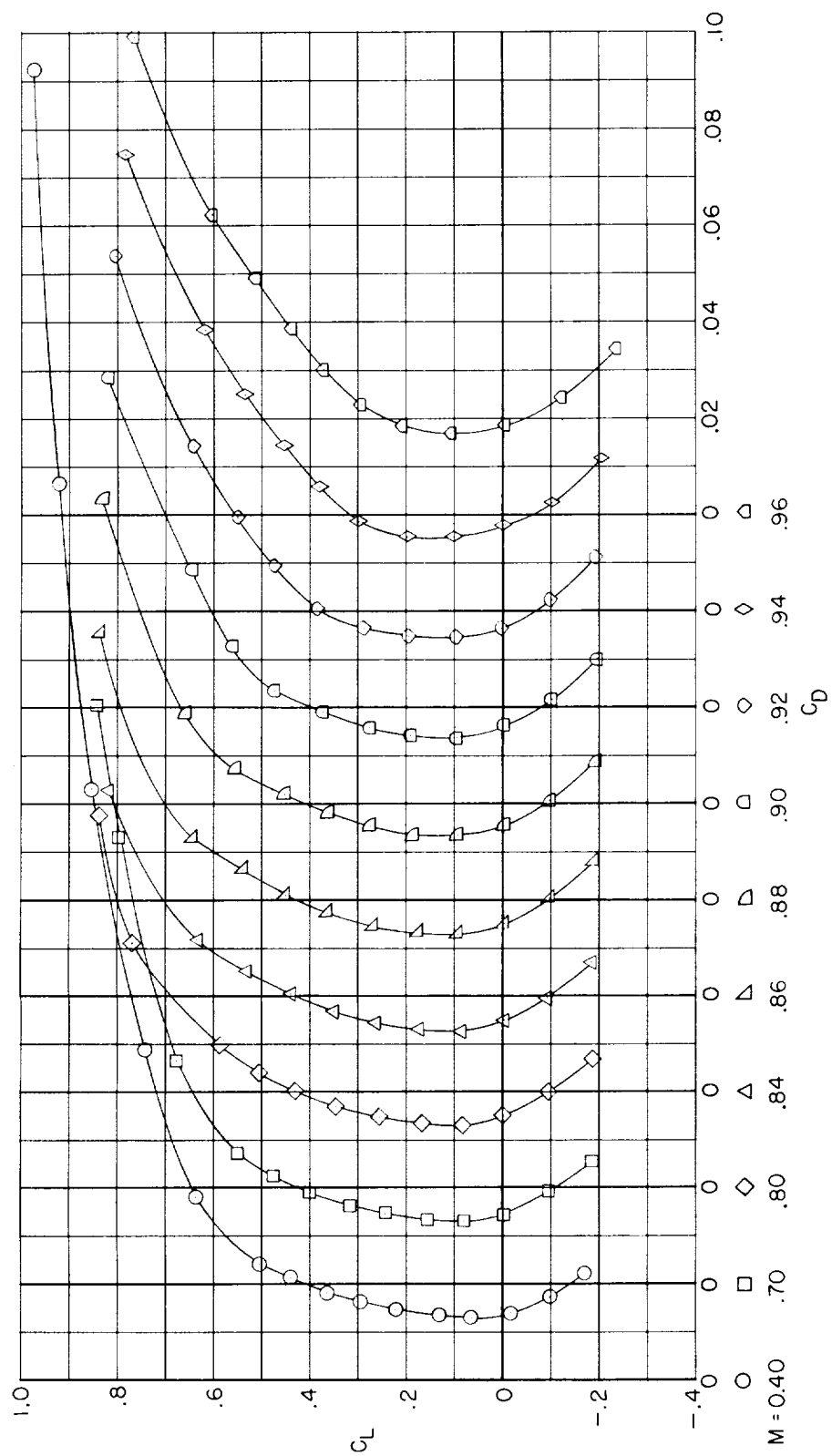


Figure 13.- Variation with Mach number of horizontal-tail effectiveness parameter for model with contoured body, wing (modified inboard trailing edge), and vertical tail.



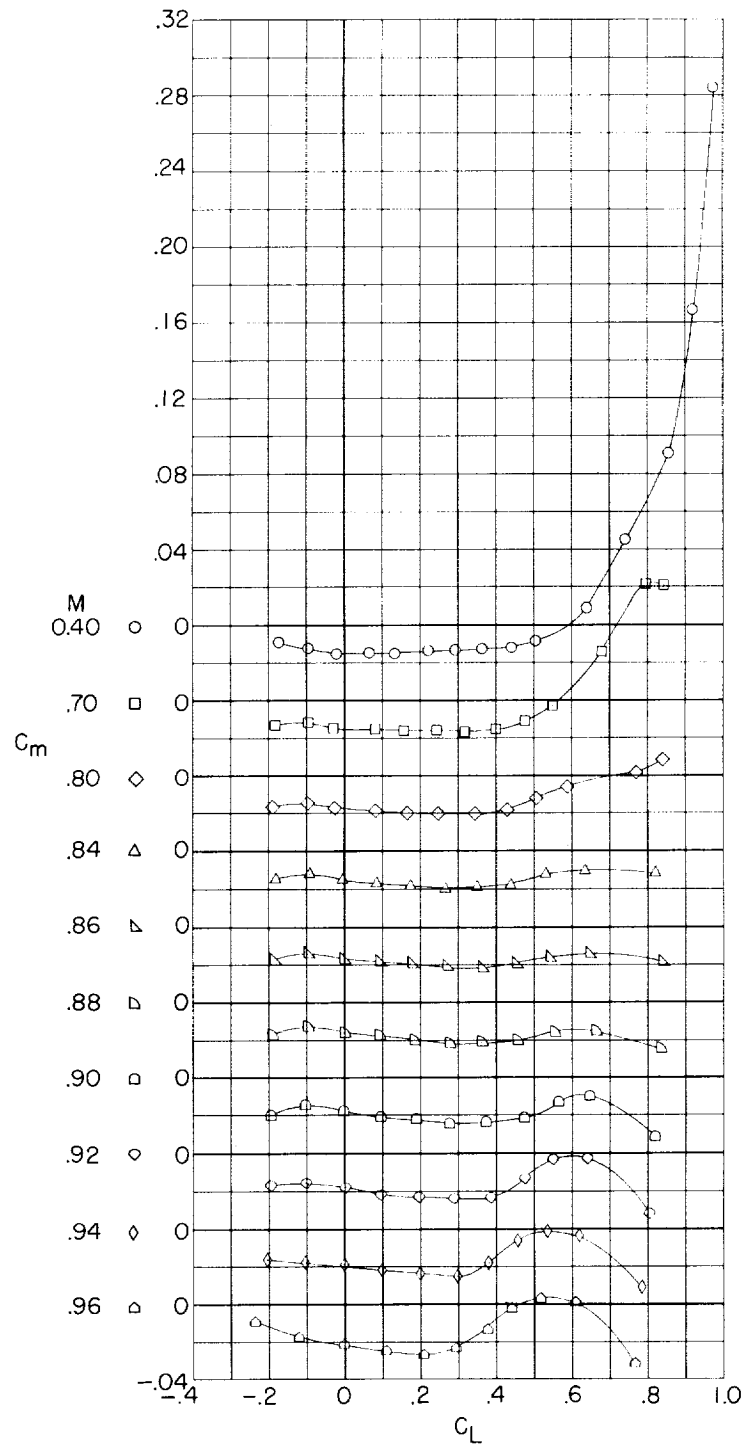
(a) Lift coefficient.

Figure 14.- Longitudinal aerodynamic characteristics of model with contoured body and wing (modified inboard trailing edge).



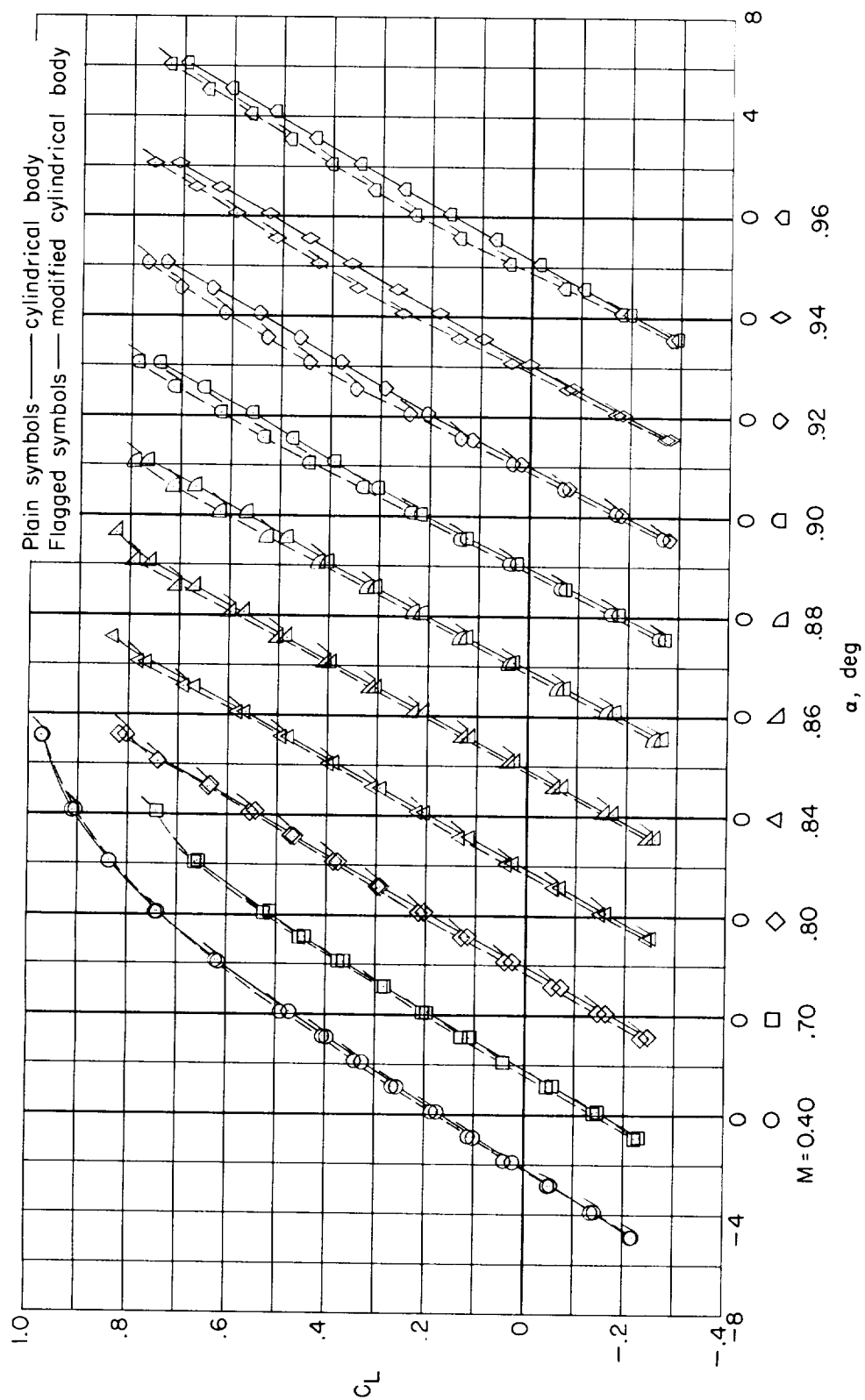
(b) Drag coefficient.

Figure 14.- Continued.



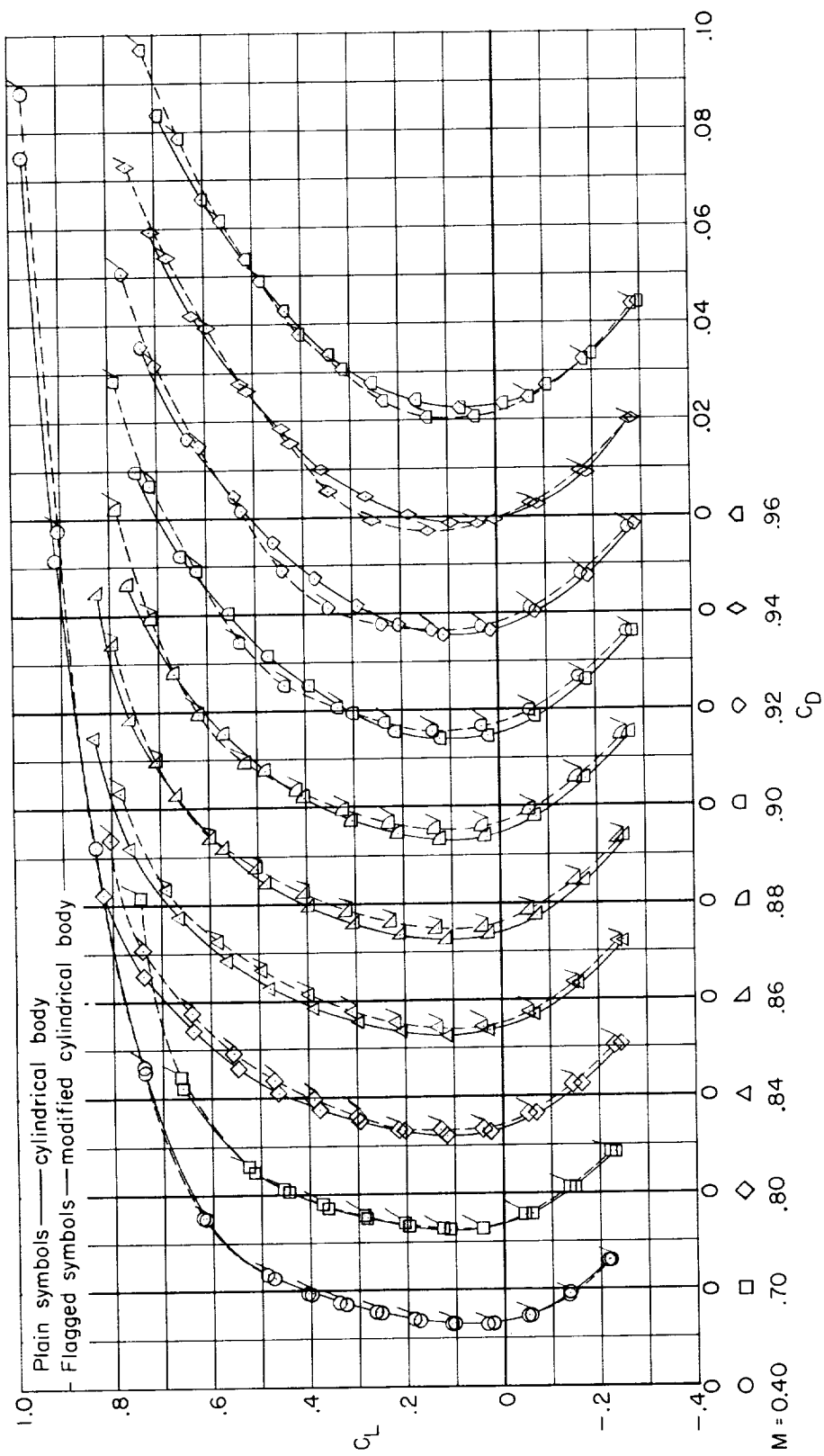
(c) Pitching-moment coefficient.

Figure 14.- Concluded.



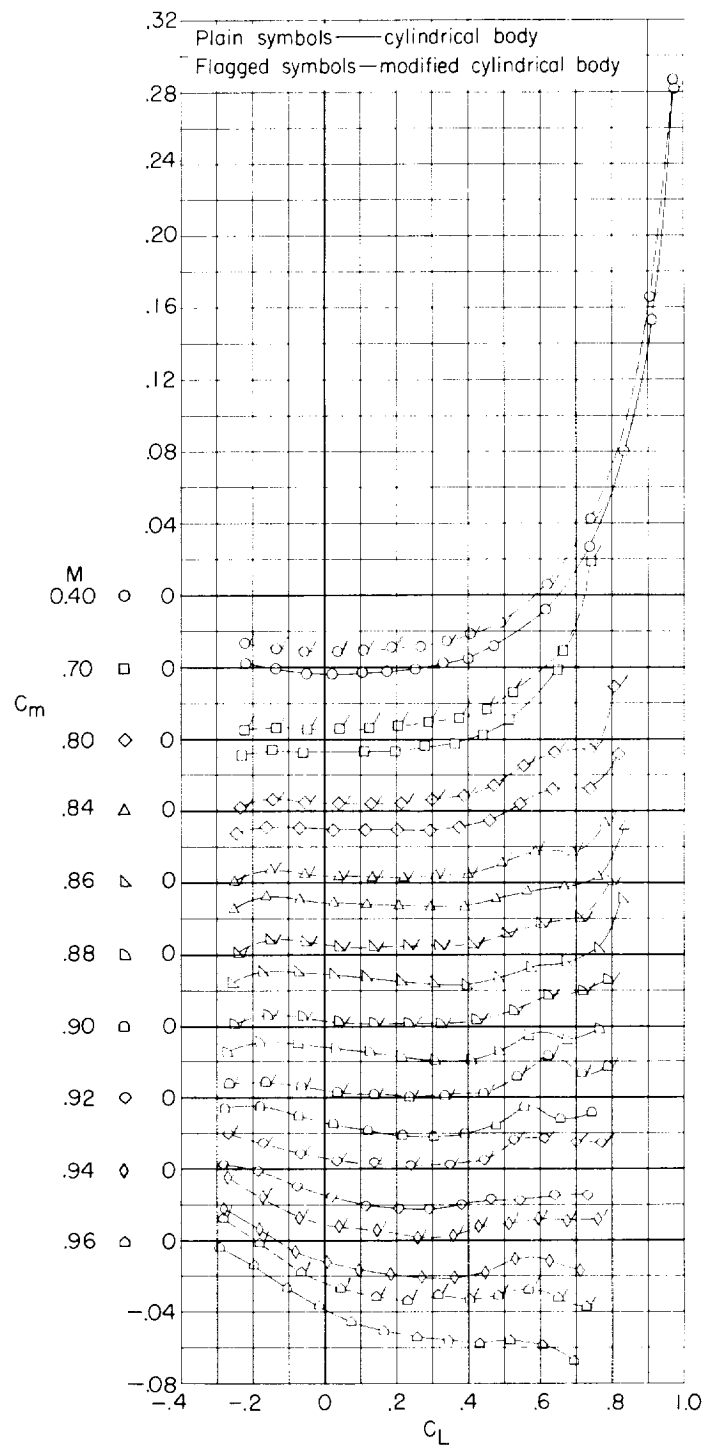
(a) Lift coefficient.

Figure 15.- Longitudinal aerodynamic characteristics of model with cylindrical and modified cylindrical bodies and wing (modified inboard trailing edge).



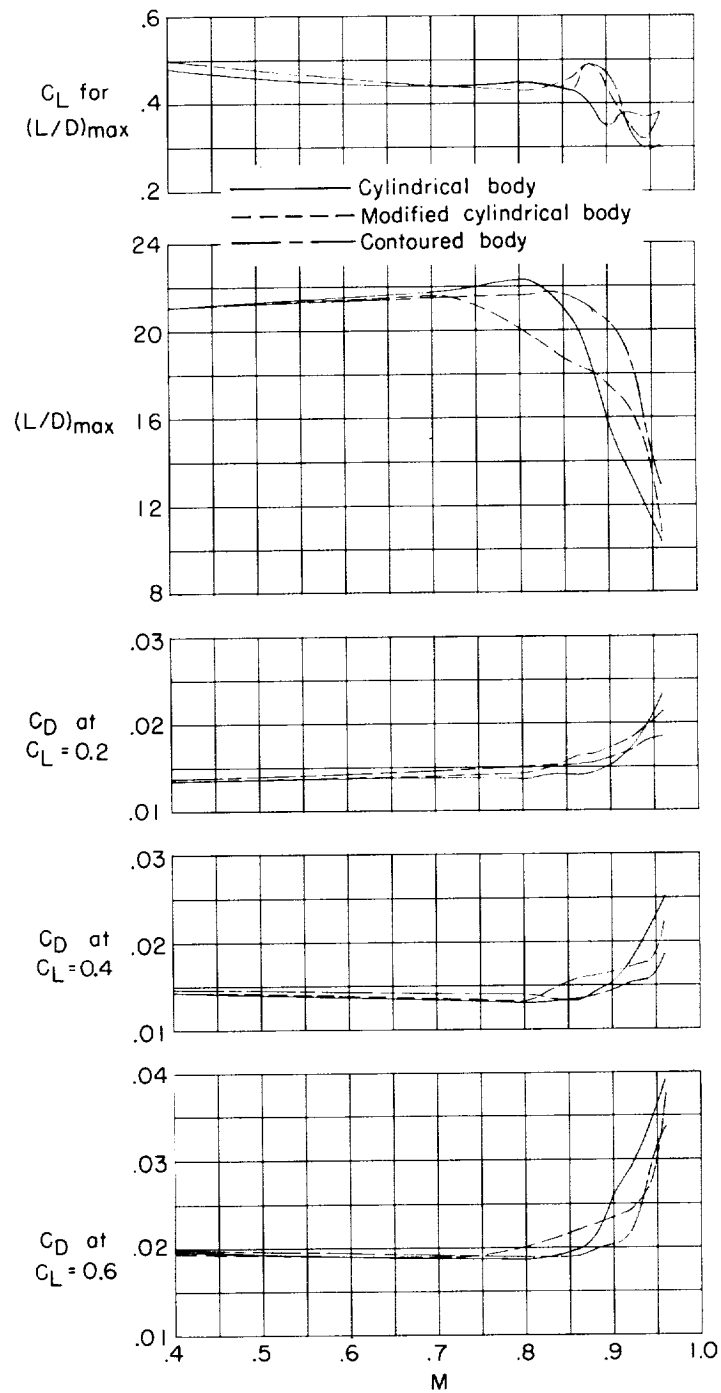
(b) Drag coefficient.

Figure 15.- Continued.



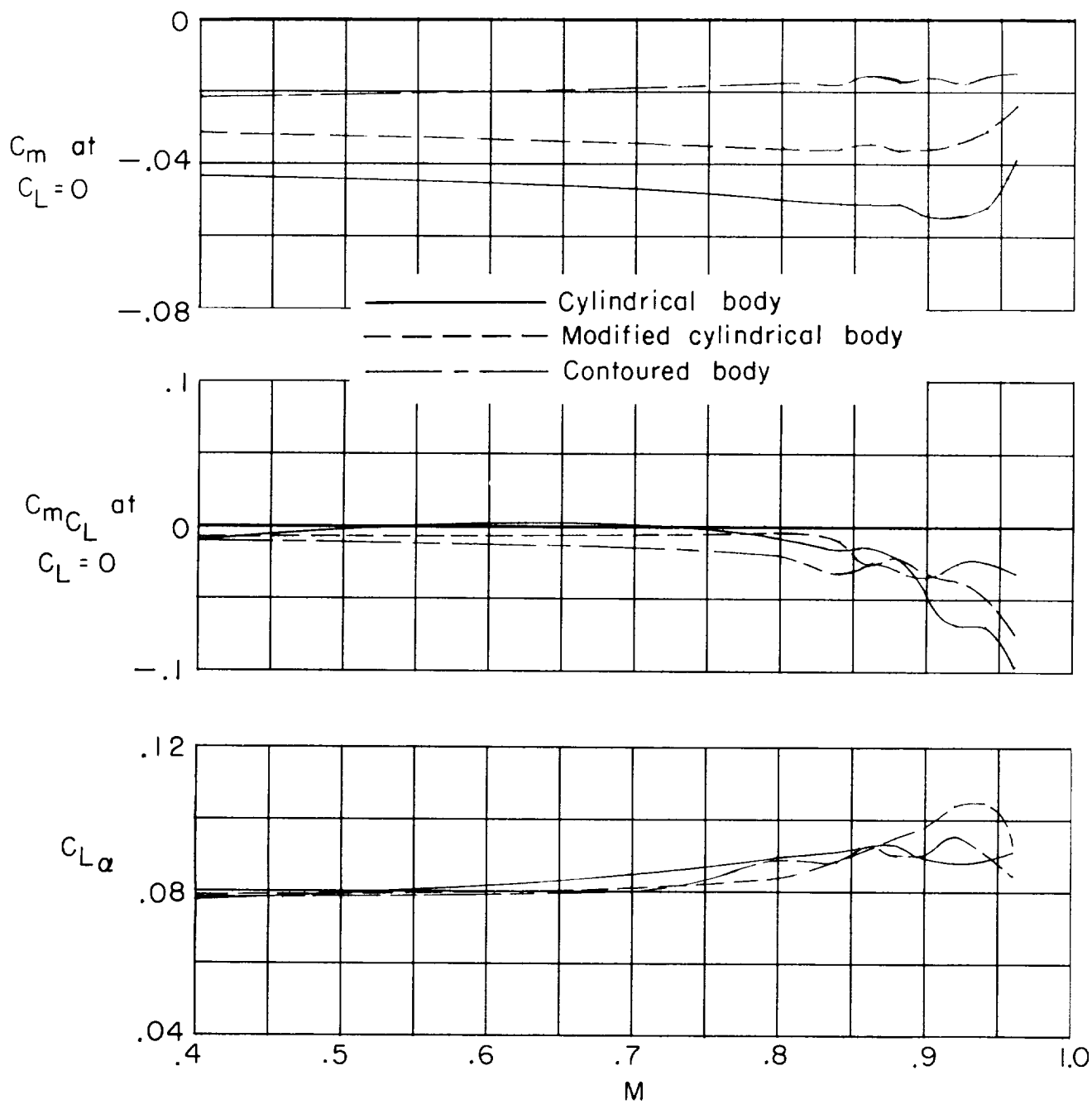
(c) Pitching-moment coefficient.

Figure 15.- Concluded.



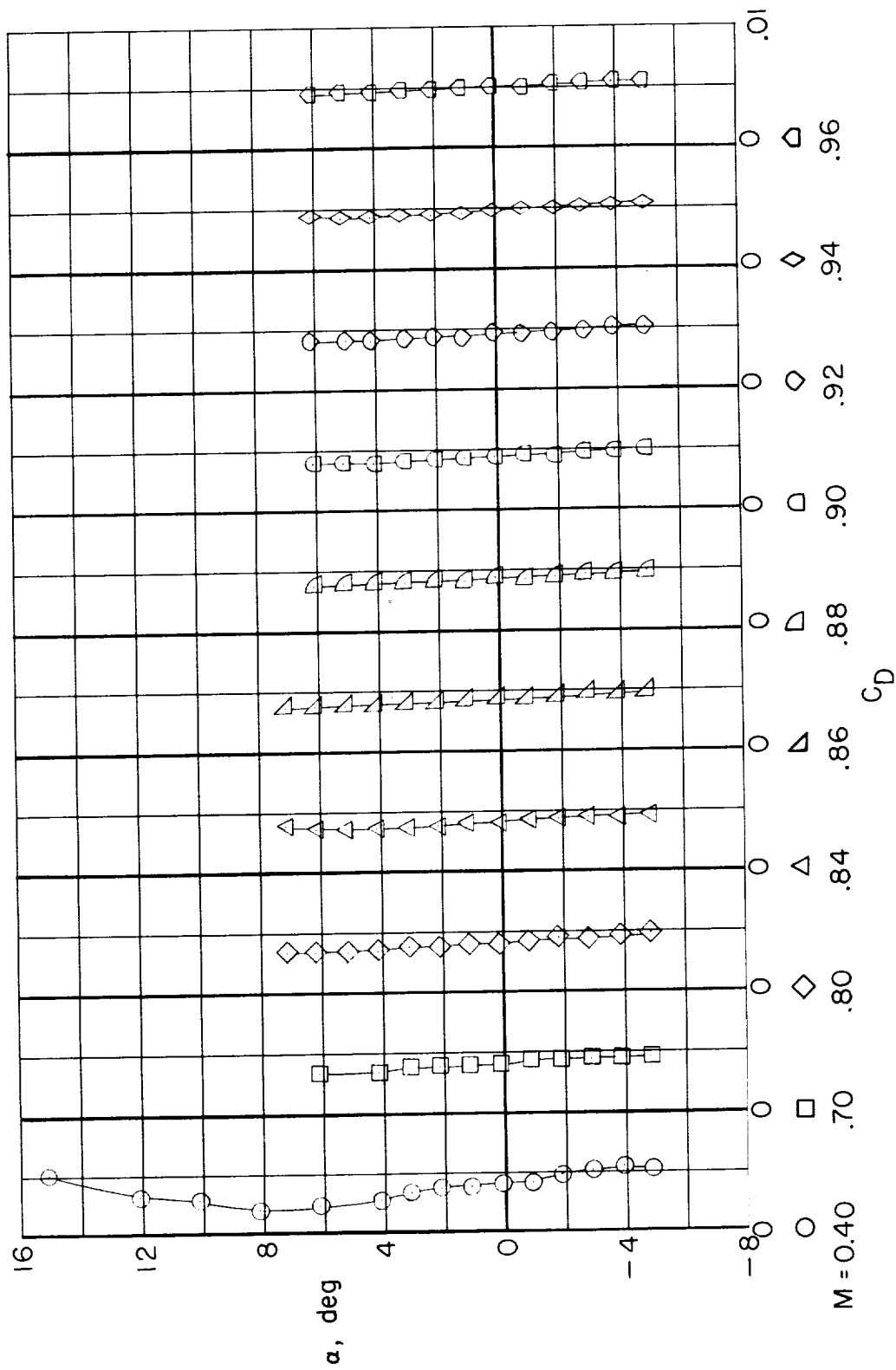
(a) C_L for $(L/D)_{max}$; $(L/D)_{max}$; C_D .

Figure 16.- Variation with Mach number of longitudinal aerodynamic characteristics of model with wing (modified inboard trailing edge) and three body configurations.



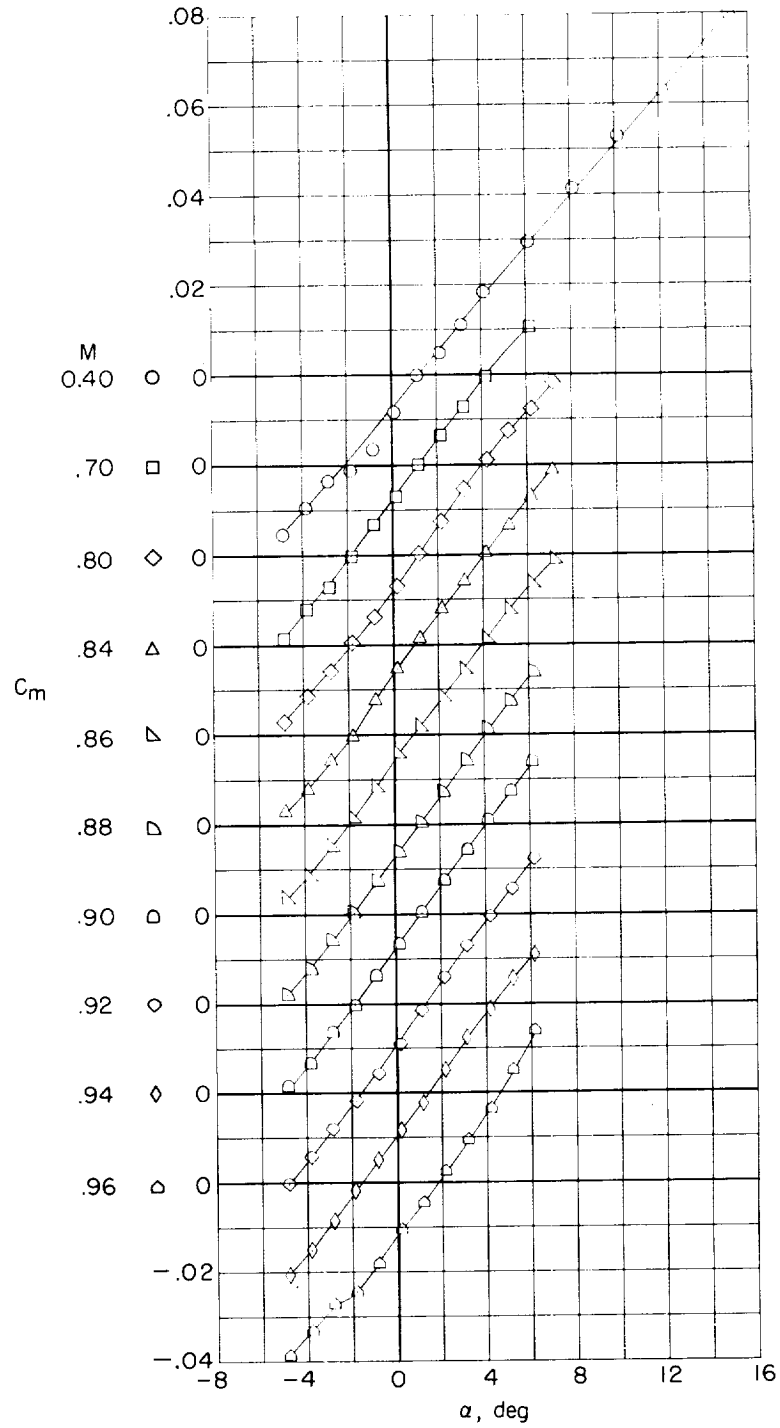
(b) C_m at $C_L = 0$; C_{mC_L} at $C_L = 0$; $C_{L\alpha}$.

Figure 16.- Concluded.



(a) Drag coefficient.

Figure 17.- Longitudinal aerodynamic characteristics of cylindrical body.



(b) Pitching-moment coefficient.

Figure 17.- Concluded.

